Corresponding authors.
Eelco J. Rohling: eelco.rohling@anu.edu.au;
Fiona D. Hibbert: fiona.hibbert@anu.edu.au

Title.

Asynchronous Antarctic and Greenland ice-volume contributions to the last interglacial sea-level highstand

Author List.

Eelco J. Rohling [a,b*], Fiona D. Hibbert [a*], Katharine M. Grant [a], Eirik V. Galaasen[c], Nil Irvalı[c], Helga F. Kleiven[c], Gianluca Marino[a,d], Ulysses Ninnemann[c], Andrew P. Roberts[a], Yair Rosenthal[e], Hartmut Schulz[f], Felicity H. Williams[a], Jimin Yu[a]

[a.] Research School of Earth Sciences, The Australian National University, ACT 2601, Canberra, Australia.
[b.] Ocean and Earth Science, University of Southampton, National Oceanography Centre, Southampton SO14 3ZH, United Kingdom.
[c.] Department of Earth Science and Bjerknes Centre for Climate Research, University of Bergen, Allegaten 41, 5007 Bergen, Norway
[d.] Department of Marine Geosciences and Territorial Planning, University of Vigo, 36310 Vigo, Spain.
[e.] Institute of Marine and Coastal Sciences, Rutgers University, New Brunswick, New Jersey 08903, USA.
[f.] Department of Geology and Paleontology, University of Tuebingen, Sigwartstrasse 10, D-7400, Tuebingen, Germany.
* = These authors contributed equally to this work.

The last interglacial (LIG; ~130 to ~118 thousand years ago, ka) was the last time global sea level rose well above the present level. Greenland Ice Sheet (GrIS) contributions were insufficient to explain the highstand, so that substantial Antarctic Ice Sheet (AIS) reduction is implied. However, the nature and drivers of GrIS and AIS reductions remain enigmatic, even though they may be critical for understanding future sea-level rise. Here we complement existing records with new data, and reveal that the LIG

contained an AIS-derived highstand from ~129.5 to ~125 ka, a lowstand centred on 125-124 ka, and joint AIS+GrIS contributions from ~123.5 to ~118 ka. Moreover, a dual substructure within the first highstand suggests temporal variability in the AIS contributions. Implied rates of sea-level rise are high (up to several meters per century; m c^{-1}), and lend credibility to high rates inferred by ice modelling under certain ice-shelf instability parameterisations.

Introduction

The magnitudes and rates of mass-reductions in today's remaining ice sheets (GrIS and AIS) in response to (past or future) warming beyond pre-industrial levels remain poorly understood. With sea levels reaching a highstand of +6 to +9 m[1,2,3], or up to 2 m higher[4], relative to the present (hereafter 0 m), the LIG is a critical test-bed for improving this understanding. Thermosteric and mountain glacier contributions fell within 0.4±0.3 m and at most 0.3±0.1 m, respectively[5,6] , and also Greenland Ice Sheet (GrIS) contributions were insufficient to explain the LIG highstand[7,8,9]. Hence, substantial Antarctic Ice Sheet (AIS) reduction is implied[1,2,3]. Determining AIS and GrIS sea-level contributions during the LIG in more detail requires detailed records with tightly constrained chronologies, along with statistical and model-driven assessments [e.g.,1,2,3,9,10,11,12,13,14,15] (*Supplementary Note 1)*. To date, however, chronological (both absolute and relative) and/or vertical uncertainties in LIG sea-level data have obscured details of the timings, rates, and origins of change.

Age control is most precise for radiometrically dated coral-based sea-level data, but stratigraphically discontinuous LIG coverage of these complex 3-dimensional systems, and species- or region-specific habitat-depth uncertainties affect the inferred sea-level estimates[11]. Stratigraphic coherence and, therefore, relative age-relationships among samples are stronger in the sediment-core-based Red Sea relative sea-level (RSL) record[1,10,16,17,18] (*Methods*), but its LIG signals initially lacked replication and sufficient age control[1,17]. Chronological alignment of the Red Sea record with radiometrically dated speleothem records has since settled its age for the LIG-onset [10,18,19] , but the LIG-end remains poorly constrained (*Methods*). Also, the Red Sea record has since 2008[Ref.1] been a statistical stack of several records without the tight sample-to-sample stratigraphy of contiguous sampling through a single core, and this has obscured details that are essential for studying centennial-scale changes[10,17,18,19]. Advances in understanding LIG sea-level contributions therefore relied on statistical deconvolutions based on multiple datasets and associated evaluations with ambiguous combining of chronologies[2,12,13,20] , or considered only mean LIG contributions[21]. Some of these studies suggest that AIS contributions likely

preceded GrIS contributions, and that there were intra-LIG sea-level fluctuations, with kilo-year averaged rates of at most 1.1 m per century (and likely smaller)[13], though this does not discount higher values for centennial-scale averages[e.g.,1]. To quantify centennial-scale average sea-level-rate estimates that may reveal rapid events and processes of relevance to the future, and robustly distinguish AIS from GrIS contributions, we present an approach that integrates precise event-dating from coral/reef and speleothem records[3,22,23,24] with stratigraphically tightly constrained Red Sea sea-level records and a broad suite of palaeoceanographic evidence. Results indicate that the LIG contained an early AIS-derived highstand, followed by a drop centred on 125-124 ka, and then joint AIS+GrIS contributions for the remainder of the LIG. We Infer high rates of sea-level change (up to several meters per century; m c^{-1}), likely reflecting complex interactions between oceanic warming, dynamic mass loss, and glacio-isostatic responses.

Results

Overview of LIG sea-level evidence

The nature of LIG sea-level variability remains strongly debated, with emphasis on two issues. First, near-field sites (close to the ice sheets) in NW Europe suggest LIG sea-level stability, although study resolutions and age control remain limited and other N European sites might support sea-level fluctuations[25]. Second, there is a wealth of global sites (mostly in the far field relative to the ice sheets) that implies LIG sea-level variability (Figure 1), but which also reveals a striking divergence between site-specific signals with respect to both timing and amplitude of variability (*Supplementary Note 1*). This suggests that individual sites are overprinted by considerable site-specific influences—e.g., prevailing isostatic, tectonic, physical, biological, biophysical, and biochemical characteristics—rather than reflecting only global sea-level changes. Regardless, a more coherent pattern seems to be emerging from the more densely dated and stratigraphically well-constrained sites, which include the Seychelles, Bahamas, and also Western Australia (*Supplementary Note 1 synthesis*). The Seychelles coral data are radiometrically precisely dated, avoid glacio-isostatic offsets among sites, and include stratigraphic relationships that unambiguously reveal

relative event timings[3,22]. The Bahamas data comprise stratigraphically well-documented and dated evidence of different reef-growth phases[23]. Nevertheless, the overall coral-based literature suggests at least two plausible types of LIG history (early *versus* late highstand solutions) that remain to be reconciled (*Supplementary Note 1, synthesis*).

Updated Red Sea age model

Regarding the Red Sea RSL record, we improve its LIG-end age control[10,18] by comparing the entire dataset (the stack) with radiometrically dated coral-data compilations[11,16] and Yucatan cave-deposits that indicate when sea level dropped below the cave (i.e., a "ceiling" for sea level)[24]. This comparison reveals that the 95% probability limit of the Red Sea stack on its latest chronology[10,19] dropped too early (123 ka; see *Methods* and *Supplementary Note 2*) relative to the well-dated archives (119-118 ka; Figure 2b,c; *Supplementary Figures 2 and 3*). We, therefore, adjust this point to 118.5±1.2 ka (95% uncertainty bounds) (Figure 2, *Supplementary Figures 2 and 3*), and accordingly revise all interpolated LIG ages with fully propagated uncertainties (*Supplementary Figure 2*).

Estimates of Greenland mass loss

Next, we compare the Red Sea sea-level information (Figures 2b,c,e,f) with estimates of GrIS-derived LIG sea-level contributions from a model-data-assimilation of Greenland ice-core data for summer temperature anomalies, accumulation rates, and elevation changes[9] (Figure 2a). We add independent support for the inferred late GrIS contribution[9], based on a newly extended record of sea-water oxygen isotope ratios ($\delta^{18}O_{sw}$) from a sediment core from Eirik Drift, off southern Greenland. In this location, $\delta^{18}O_{sw}$ reflects Greenland meltwater input with a sensitivity of 4 ± 1.2 m global sea-level rise for the –1.3 ‰ change seen in the $\delta^{18}O_{sw}$ record from ~128 to ~118 ka (Figure 2a) (*Methods, Supplementary Note 3*). This record suggests (albeit within combined uncertainties) generally somewhat lower GrIS contributions than Yau et al.[9], which may agree with results from other modelling studies for GrIS[14,15]. Both the modelling and $\delta^{18}O_{sw}$ approaches indicate a late GrIS contribution to LIG sea level, which is further supported by wider N. Atlantic and European

141 palaeoclimate data, which reveal that contributions started after 127 ka, while
142 GrIS started to regain net mass from 121 ka[27].
143
144 ***AIS and GrIS distinction***
145 Although GrIS did not affect LIG sea-level change significantly before 126.5-127
146 ka (Figure 2a), the Red Sea and coral data compiled here imply that sea level
147 crossed 0 m at 130-129.5 ka, during a rapid rise to a first highstand apex that
148 was reached at ~127 (Figure 2b,c,e,f). The Seychelles record indicates
149 specifically that sea level reached 5.9 ±1.7 m by 128.6 ±0.8 ka[3]. We infer that
150 both the first LIG rise above 0 m, and the subsequent rapid rise between 129.5-
151 127 ka, resulted from AIS reduction. Similar qualitative inferences about an
152 early-LIG AIS highstand contribution have been made previously[3,9,19], including
153 attribution to sustained heat advection to Antarctica during Heinrich Stadial 11
154 (HS11; 135-130 ka)[19], when a northern hemisphere deglaciation pulse (~70 m
155 sea-level rise in 5,000 years) caused overturning-circulation shutdown[28], a
156 widespread North Atlantic cold event, and southern hemisphere warming
157 (Figure 2d). Here we present a quantitative AIS and GrIS separation with
158 comprehensively evaluated uncertainties.
159
160 First, we determine centennial-scale LIG sea-level variability from the
161 continuous (and contiguous) single-core RSL record of central Red Sea core KL11
162 on our new Red Sea LIG age model. We validate this record with new data for
163 high-accumulation-rate core KL23 from the northern Red Sea; i.e., from a
164 physically separate setting than KL11 (*Methods*) (Figure 2e). Given this
165 validation, we continue with KL11 alone because it remains the most detailed
166 record from the best-constrained (central) location in the Red Sea RSL
167 quantification method, where $\delta^{18}O$ is least affected by either Gulf of Aden inflow
168 effects in the south, or northern Red Sea convective overturning and
169 Mediterranean-derived weather systems in the north[16,29].
170
171 Second, we perform a Monte Carlo (MC)-style probabilistic analysis of the KL11
172 record (Figure 2f), which accounts for all uncertainties in individual-sample RSL
173 and age estimates (cf. blue cross in Figure 2e). This procedure mimics that

applied previously to the Red Sea stack[10,18] , but now contains an additional criterion of strict stratigraphic coherence (*Methods*). The analysis leads to statistical uncertainty reduction based on data-point characteristics, density, and stratigraphy. Remaining RSL uncertainties are ±2.0 to 2.5 m for the 95% probability zone of the probability maximum (PM, modal value; Figure 2f; *Methods*).

Both PM and median reveal an initial RSL rise from ~129.5 to ~127 ka to a highstand apex centred on ~127 ka, followed by a drop to a lowstand centred on 125-124 ka at a few metres below 0 m, and then a small return to a minor peak above 0 m at ~123 ka (Figure 2f). To quantify AIS contributions, we apply a first-order glacio-isostatic correction (with uncertainties) to translate the record from RSL to global mean sea level (GMSL) (*Supplementary Note 4*) (Figure 3a), and then subtract the GrIS-contribution records (Figures 2a, 3b). Our results quantify significant asynchrony and amplitude-differences between GrIS and AIS ice-volume changes during the LIG (Figure 3b,c). A caveat applies in intervals where the reconstructed AIS sea-level record drops below –10m, because at that stage the maximum AIS growth limit is approximated (AIS growth is limited by Antarctic continental shelf edges). Whenever the reconstructed AIS sea-level record falls below –10m (notably after ~119 ka), North American and/or Eurasian ice-sheet growth contributions likely became important. This timing agrees with a surface-ocean change south of Iceland from warm to colder conditions[27].

Intra-LIG sea-level variability

Red Sea intra-LIG variations are generally consistent (within uncertainties) in timing with apparent sea-level variations in the well-dated and stratigraphically coherent coral data from the Seychelles, Bahamas[3,22,23], but with larger amplitudes. Northwestern Red Sea reef and coastal-sequence architecture reconstructions offer both timing and amplitude agreement (although age control needs refining)[30,31] (*Supplementary Note 1*). The reef-architecture study in particular[30] indicates an early-LIG sea-level rise with a post-128-ka

culmination at 5-10 m above present, followed by a millennial-scale ~10 m sea-level drop to a lowstand centred on ~124 ka.

In more detail, the probabilistic Red Sea record suggests a statistically robust dual substructure within the initial LIG sea-level rise (Figure 2f), which is replicated between Red Sea records (Figure 2e). It is not (yet) supported in wider global evidence (*Methods, Supplementary Note 1*), but there are indications that certain systems may have recorded it independently. For example, southwestern Red Sea reef-architecture reveals two main reef phases with a superimposed minor patch-reef phase[1,32], reaching total thicknesses up to 10 m. But more precise dating and support from other locations are needed to be conclusive. In this context, we calculate with a basic fringing-reef accretion model that the rapid rises and short highstands inferred here (Figure 2e,f) may have left limited expressions in reef systems, except for rare ones with exceptionally high accretion rates, or where rapid crustal uplift offset some of the rapid sea-level rises (*Supplementary Note 5*). Hence, we consider wider palaeoceanographic evidence to evaluate the suggested sea-level history.

Palaeoceanographic support

AIS meltwater pulses implied by sea-level rises R1 and R2 (Figure 2f) should have left detectable signals around Antarctica. The early-LIG AIS sea-level contribution occurred immediately after Heinrich Stadial (HS) 11, when overturning circulation had recovered from a collapsed HS11 state (Figures 2,3,4)[28]. This likely enhanced advection of relatively warm northern-sourced deep water into the Circumpolar Deep Water (CDW), which impinges on the AIS. At the same time, there was a peak in Antarctic surface temperatures (Figures 2d,4c) and Southern Ocean sea surface temperatures (ODP Site 1094 TEX_{86}^{L}, ODP Site 1089 planktic foraminiferal $\delta^{18}O$) (Figure 4c-e), and Southern Ocean sea ice was reduced (Figure 4b). We infer that early-LIG AIS retreat resulted from both atmospheric and (subsurface) oceanic warming, which—together with minimal sea ice (important for shielding Antarctic ice shelves from warm circumpolar waters[e.g.,33])—drove enhanced subglacial melting rates and ice-

shelf destabilisation, and thus strong AIS sea-level contributions between 130 and 125 ka.

Wider palaeoceanographic evidence can be used to test the concept that major AIS melt will provide fresh water to the ocean surface, which density-stratifies the near-continental Southern ocean, impeding Antarctic Bottom Water (AABW) formation[34,35] , which in turn will lead to reduced AABW ventilation/ oxygenation and an increase in North Atlantic Deep Water (NADW) proportion versus AABW proportion in the Atlantic Ocean[28,36]. Thus, we infer strong support for early-LIG AIS melt from palaeoceanographic observations. For example, an anomaly in authigenic uranium mass-accumulation-rates (aU MAR) in Southern Ocean ODP Site 1094 has been attributed to bottom-water deoxygenation (AABW reduction/ stagnation), due to strong Antarctic meltwater releases and consequent water-column stratification[36] (Figures 3c, 4g). Also, increased bottom-water $\delta^{13}C$, due to expansion of high-$\delta^{13}C$ NADW at the expense of low-$\delta^{13}C$ AABW, occurred at the end of HS11 in both the abyssal North Atlantic (ODP Site 1063, core MD03-2664) and South Atlantic (Sites 1089 and 1094) (Figure 4i). Moreover, ε_{Nd} changes in Site 1063[28] support the $\delta^{13}C$ interpretation (Figure 4h). Given that intensification of relatively warm NADW likely plays a key role in subglacial melting and resultant AABW source-water freshening[33,37], we infer a positive feedback. In this feedback, meltwater-induced AABW reduction warmed CDW through increased admixture of relatively warm NADW, which then caused further subglacial melting and AABW source-water freshening, driving additional AABW decline. Finally, a distinct early-LIG minimum in the Site 1089 planktic-benthic foraminiferal $\delta^{18}O$ gradient indicates a persistent surface buoyancy anomaly, which agrees with strong AIS meltwater input[38] (Figure 4c-f). Surface buoyancy/stratification increase would restrict air-sea exchange and subsurface heat loss. Analogous to explanations offered for high melt rates in some regions of Antarctica today and for even higher melt rates in a warmer future climate[39], we therefore propose another positive feedback for the LIG, in which melt-stratification led to subsurface ocean warming, which then intensified ice-shelf melting.

Finally, we note that the aU MAR variations in Southern Ocean Site 1094[36] also agree in more detail with our inferred dual substructure in the AIS-related early-LIG highstand (Figure 3b,c). It is not yet possible to eliminate robustly the inferred offsets (which fall within uncertainties) between the ODP 1094 AICC2012-based chronology[36] and our LIG chronology[10,19,this study] (Figure 3b,c), but the offsets may also (partly) arise from time-lags between meltwater input at the surface and oxygenation at the sea floor. Given the position of ODP Site 1094 (South Atlantic sector), the aU MAR record may be to some extent site-specific, in which case it suggests a likely meltwater source from the West Antarctic Ice Sheet (WAIS). The lack of later aU MAR spikes for our further inferred AIS contribution may then suggest either that most of WAIS had been lost during the earliest LIG, or that it had at least retreated far enough to stop contributions as is also indicated by ice-sheet studies[14,40,41,42,43].

Discussion

The summarised suite of palaeoceanographic observations offers strong support to our reconstruction that early-LIG sea-level rise above 0 m derived from the AIS, and that this meltwater input occurred in several distinct pulses. Interruption of the rapid AIS mass-loss rate during the main phase of ice-sheet/shelf reduction may reflect negative feedbacks of isostatic rebound and resultant ice-shelf re-grounding that temporarily limited ice-mass loss[e.g.,44,45,46,47,48,49]. The sea-level-lowering rates we find in between the LIG rapid-rise events range between multi-centennial means of –0.23 and –0.63 m c^{-1} (with peaks up to –1 m c^{-1}) (Figures 2g, *Supplementary Figure10*). These imply high rates of global net ice-volume growth, but we note that LIG accumulation rates over the AIS may even have been ~30% higher than present[50] (*Supplementary Note 6*).

Our record (Figure 3a) indicates a first sea-level rise (R1) above 0 m at event-mean values of 2.8 (1.2-3.7) m c^{-1}, followed by R2 at 2.3 (0.9-3.5) m c^{-1}, and R3 at 0.6 (0.1-1.3) m c^{-1}, where the ranges in brackets reflect the 95% probability bounds. These values lend credibility to similar rates inferred from ice modelling that includes certain ice-shelf hydrofracturing and ice-cliff collapse

304 paramerisations[51]. These processes remain debated, but the apparent reality of
305 such extreme rates in pre-anthropogenic times—when climate forcing was
306 slower, weaker, and more hemispherically asynchronous than today—increases
307 the likelihood that such poorly understood mechanisms may be activated under
308 anthropogenic global warming, to yield extreme sea-level rise.
309
310 In conclusion, we have reconstructed (Figure 3) an initial sea-level highstand
311 (above 0 m) at ~129.5 to ~124.5 ka, which derived almost exclusively from the
312 AIS (in agreement with palaeoceanographic evidence), and which reached its
313 highstand apex at around 127 ka. We find that the rise toward the apex occurred
314 in two distinct phases, which also agrees with a palaeoceanographic record of
315 AABW ventilation changes. Following the apex at ~127 ka, we reconstruct a sea-
316 level drop to a relative lowstand centred on 125-124 ka, which in turn gave way
317 to a minor rise toward a small peak at or just above 0 m at ~123 ka. GrIS
318 contributions were differently distributed through time. These contributions
319 slowly ramped up from ~127 ka onward, reaching maximum, sustained
320 contributions to LIG sea level from ~124 ka until the end of the LIG. Thus, we
321 quantitatively reconstruct that there was strong asynchrony in the AIS and GrIS
322 contributions to the LIG highstand, with an AIS-derived maximum that spanned
323 from ~129.5 to ~124.5 ka, a low centred on 125-124 ka, and variable, joint
324 AIS+GrIS influences from ~124 to ~119 ka.
325
326 We observe rapid rates of sea-level change within the LIG. These may reflect
327 complex interactions through time between: (a) enhanced accumulation during a
328 regionally warmer-than-present interglacial[50]; (b) persistent dynamic ice-loss
329 due to long-term heat accumulation[e.g.,19]; (c) negative glacio-isostatic feedbacks
330 to ice-mass loss[e.g., 44,45,46,47,48,49]; and (d) positive oceanic feedbacks to Antarctic
331 meltwater releases (*Discussion*, and Refs.52,35). Similar sequences may develop
332 in future, given that warmer CDW is encroaching onto Antarctic shelves, so that
333 future sea-level rise may become driven by increasingly rapid mass-loss from the
334 extant AIS ice sheet[e.g., 53,54,55,56], in addition to the well-observed GrIS
335 contribution[e.g., 57,58].
336

Finally, we infer intra-LIG sea-level rises with event-mean rates of rise of 2.8 m c^{-1}, 2.3 m c^{-1}, and 0.6 m c^{-1}. Such high pre-anthropogenic values lend credibility to similar rates inferred from some ice-modelling approaches[51]. The apparent reality of such extreme pre-anthropogenic rates increases the likelihood of extreme sea-level rise in future centuries.

Methods

Red Sea relative sea level record

The Red Sea relative sea-level (RSL) record derives from contiguous sampling of sediment cores and, thus, has tighter stratigraphic control than samplings of reef systems, which consist of more complex 3-dimensional frameworks. Red Sea sediment cores consist of beige to dark brown hemipelagic mud and silt, with high wind-blown dust contents in glacial/cold intervals and lower wind-blown dust contents in interglacial intervals. This results in colour and sediment-geochemistry variations that allow straightforward assessment of bioturbation. This was found to be very limited in the cores used here, which agrees with extremely low numbers of benthic microfossils (benthic numbers per gram are an order of magnitude, or more, lower than planktonic numbers per gram[59], reaching two orders of magnitude lower in the LIG[60]), which in turn agree with extremely low Total Organic Carbon contents (at or below detection limit)[60]. With limited bioturbation, the stratigraphic coherence of the sediment record is well preserved.

The new KL23 $\delta^{18}O$ analyses were performed on 30 specimens per sample of the planktonic foraminifer *Globigerinoides ruber* (white) from the 320 to 350 μm size fraction. Sample spacing and KL11-equivalent age model are indicated in the data file. Prior to analysis, foraminiferal tests were crushed and cleaned by brief ultrasonication in methanol. Measurements were performed at the Australian National University using a Thermo Scientific DELTA V Isotope Ratio Mass Spectrometer coupled with a KIEL IV Carbonate Device. Results are reported in per mil deviations from Vienna PeeDee Belemnite using NBS-19 and NBS-18

carbonate standards. External reproducibility (1σ) was always better than 0.08 ‰.

Red Sea carbonate $\delta^{18}O$ is calculated into RSL variations using a polynomial fit to the method's mathematical solution[16,29] (see Supplement of Ref. [17]). The Red Sea stack of records[17] was dated in detail through the last glacial cycle based on the U/Th dated Soreq Cave speleothem record[10]. Through the LIG, however, it was constrained only by interpolation between tie-points at 135 and 110 ka. The age-model for the LIG-onset was later validated[19], yet the LIG-end remained to be better constrained. Here we make an important adjustment for the LIG-end, based on radiometrically dated criteria described in the main text. This assignment is based on a first-order assessment of the entire Red Sea stack using a simple polynomial and its 95% uncertainty envelope, and it is validated by the fact that in the more precise probabilistic analysis of KL11 alone, the 95% probability zone for individual datapoints (lightest grey) also crosses 0 m at 118.5 ka. We only use the latter in validation, to avoid circularity in the age-model construction. This reassigns the level originally dated (by interpolation) at 123 ka in the Red Sea stack[10], to 118.5 ka with 95% uncertainty bounds of ±1.2, where the uncertainties relate to those of the original age model[10] (Figure 2, *Supplementary Figure 2*). Initial age uncertainties (at 95%) all derive from that study. Next, age interpolations using the adjusted chronological control point are performed probabilistically using a Monte-Carlo (MC)-style (n = 2000) sequence of Hermite splines that impose monotonic succession to avoid introduction of spurious age-reversals (*Supplementary Figure 2*). Our new chronology for the Red Sea LIG record implies low sediment accumulation rates without major fluctuations within the LIG (*Supplementary Figure 2*). Finally, when performing the sea-level probabilistic assessment for core KL11, we use the newly diagnosed age uncertainties from *Supplementary Figure 2*, which are wider (more conservative) through the interval 120-110 ka than the originals (*Supplementary Figure 2*).

The two separate high-resolution LIG sea-level records from the Red Sea discussed here are an existing one from central Red Sea core KL11 (18°44.5′N,

39°20.6′E)[1], and a new one from northern Red Sea core KL23 (25°44.9′N, 35°03.3′E). The new KL23 LIG record validates the KL11 record, but its early-LIG peak comprises only one sample/datapoint. The validity of this peak was confirmed with a multiple replication exercise (Figure 2e, grey).

Through its continuity, stratigraphic constraints, and consistently high signal-to-noise ratio, sea-level variations are identified in the Red Sea record with limited impacts from other factors[10,16,17,18,29]. However, the Red Sea sea-level record still is only a relative sea-level (RSL) record for the Hanish Sill, Bab-el-Mandab, and correction for glacio-isostatic influences is needed to obtain estimates of global mean sea level (GMSL) from this record (*Supplementary Note 4*). Following these corrections, we estimate AIS sea-level contributions by determining the difference between GMSL and two different estimates for the GrIS contribution (Yau et al.[9], and our Eirik Drift $\delta^{18}O_{sw}$ approach), with full propagation of the uncertainties involved (see below, and *Supplementary Note 3*).

The probabilistic analysis of the Red Sea core KL11 record (Figure 2f) follows the same approach as for the Red Sea RSL stack[10,18] , which gives similar results to an independent Bayesian approach using the same dataset[61]. The method uses the full probability distribution envelopes for both age and sea-level directions, as characterized by the mean and standard deviation per sample point (see blue cross in Figure 2e for these 1σ limits in KL11), and performs 5000 MC-style resamplings of the record. During this resampling, we here apply an additional criterion of strict stratigraphic coherence within the contiguously sampled KL11 record (allowing no age reversals during MC-resampling). The resultant suite of MC simulations is then analysed at set time-steps to identify the probability maximum (modal value, with 95% probability window that depends on how well-defined the modal value is), median, and the 16th, 84th, 2.5th and 97.5th percentiles that demarcate the 68% and 95% probability zones of the total MC-resampled distribution of individual sample points (Figure 2f). Because of the stratigraphic coherence in the KL11 record considered here, the modal value (and median) in each time-step probability distribution through the MC simulations is tightly constrained, with the mode (probability maximum)

typically defined within 95% bounds of only +/-2 to 2.5 m. In the earlier studies for the Red Sea stack[10,18] , this was +/-6 m, because a stack of different records does not preserve strict stratigraphic coherence from one datapoint to the next, so that relative age uncertainties between datapoints remained much larger than in our new record.

Eirik Drift surface sea-water $\delta^{18}O$ record ($\delta^{18}O_{sw}$)

Our Eirik Drift surface sea-water $\delta^{18}O$ record ($\delta^{18}O_{sw}$) was determined for core MD03-2664 (57°26'N, 48°36'W, 3442 m) using the palaeotemperature equation of Ref. [62], with a Vienna PeeDee Belemnite to Standard Mean Ocean Water standards conversion of 0.27‰, using $\delta^{18}O$[63] and Mg/Ca temperature data[64] for the planktonic foraminiferal species *Neogloboquadrina pachyderma* (sinistral; 150 to 250 μm size fraction), on the chronology of Ref. [65]. Previously published estimates for $\delta^{18}O_{sw}$ covered only late MIS 6 and early MIS 5e (2600 to 2850 cm core depth[63]), and are supplemented here with new estimates for core depths ranging between 2350 and 2600 cm. Even today, the location of MD03-2664 is dominated by currents carrying admixtures of ^{16}O-enriched Greenland melt water, with increased melt admixtures causing more negative $\delta^{18}O_{sw}$ values[66,67]. Specifically, $\delta^{18}O_{sw}$ at this site is highly sensitive to changes in the net freshwater $\delta^{18}O$ endmember[67]. Less GrIS meltwater discharge and relative dominance of sea-ice meltwater yield a less negative net freshwater endmember $\delta^{18}O$, whereas the opposite yields a very negative net freshwater endmember $\delta^{18}O$[67, and references therein]. Regional freshwater endmember changes span a range of ~10‰ or more, so while marine endmember changes are <0.5‰[67], sustained MD03-2664 $\delta^{18}O_{sw}$ changes reflect net freshwater component changes, and therefore mainly GrIS melt. Using an endmember mixing model, and fully propagating generous uncertainties, we find that (all else being constant) the observed –1.3‰ $\delta^{18}O_{sw}$ change in MD03-2664 corresponds to 4 ± 1.2 m GrIS-derived sea-level rise (*Supplementary Note 3*).

Data Availability

The new Red Sea KL23 $\delta^{18}O$ and sea level data, Eirik Drift $\delta^{18}O_{sw}$ data supporting the findings of this study, and source data for figures 2 and 3, are provided with

the paper as a Source Data file [http://doi.org/ 10.6084/m9.figshare.9790844] and via http://www.highstand.org. Further information is available from the corresponding author upon reasonable request.

References

[1] Rohling, E. J. *et al*. High rates of sea-level rise during the last interglacial period. *Nature Geosci.* **1**, 38–42, doi:10.1038/ngeo.2007.28 (2008).

[2] Kopp, R. E., Simons, F. J., Mitrovica, J. X., Maloof, A. C. & Oppenheimer, M. Probabilistic assessment of sea level during the last interglacial stage. *Nature* **462**, 863–867, doi:10.1038/nature08686 (2009).

[3] Dutton, A., Webster, J. M., Zwartz, D., Lambeck, K. & Wohlfarth, B. Tropical tales of polar ice: evidence of Last Interglacial polar ice sheet retreat recorded by fossil reefs of the granitic Seychelles islands. *Quat. Sci. Rev.* **107**, 182–196, doi:10.1016/j.quascirev.2014.10.025 (2015).

[4] Rohling, E. J. *et al*. Differences between the last two glacial maxima and implications for ice-sheet, $\delta^{18}O$, and sea-level reconstructions. *Quat. Sci. Rev.* **176**, 1–28, doi:10.1016/j.quascirev.2017.09.009 (2017).

[5] McKay, N. P., Overpeck, J. T. & Otto-Bliesner, B. L. The role of ocean thermal expansion in Last Interglacial sea level rise. *Geophys. Res. Lett.* **38**, L14605, doi: 10.1029/2011GL048280 (2011).

[6] Farinotti, D. *et al.* A consensus estimate for the ice thickness distribution of all glaciers on Earth. *Nat. Geosci.* **12**, 168–173 doi: 10.1038/s41561-019-0300-3 (2019).

[7] Cuffey, K. M. & Marshall, S. J. Substantial contribution to sea-level rise during the last interglacial from the Greenland ice sheet. *Nature* **404**, 591–594, doi:10.1038/35007053 (2000).

[8] Dahl-Jensen, D. *et al*. Eemian interglacial reconstructed from a Greenland folded ice core. *Nature* **493**, 489–494, doi:10.1038/nature11789 (2013).

[9] Yau, A. M., Bender, M. L., Robinson, A. & Brook, E. J. Reconstructing the last interglacial at Summit, Greenland: insights from GISP2. *Proc. Natl. Acad. Sci. USA* **113**, 9710–9715, doi:10.1073/pnas.1524766113 (2016).

[10] Grant, K. M. *et al*. Rapid coupling between ice volume and polar temperature over the past 150,000 years. *Nature* **491**, 744–747, doi:10.1038/nature11593 (2012).

[11] Hibbert, F. D. *et al*. Coral indicators of past sea-level change: a global repository of U-series dated benchmarks. *Quat. Sci. Rev.* **145**, 1–56, doi:10.1016/j.quascirev.2016.04.019 (2016).

[12] Düsterhus, A., Tamisiea, M. E. & Jevrejeva, S. Estimating the sea level highstand during the last interglacial: a probabilistic massive ensemble approach. *Geophys. J. Int.* **2**, 900–920, doi:10.1093/gji/ggw174 (2016).

[13] Kopp, R. E., Simons, F. J., Mitrovica, J. X., Maloof, A. C. & Oppenheimer, M. A probabilistic assessment of sea level variations within the last interglacial stage. *Geophys. J. Int.* **193**, 711–716 doi: 10.1093/gji/ggt029 (2013).

[14] Goelzer, H., Huybrechts, P., Marie-France, L. & Fichefet, T. Last Interglacial climate and sea-level evolution from a coupled ice sheet-climate model. *Clim. Past* **12**, 2195–2213 doi: 10.5194/cp-12-2195-2016 (2016).

[15] Calov, R., Robinson, A., Perrette, M. & Ganopolski, A. Simulating the Greenland ice sheet under present-day and palaeo constraints including a new discharge parameterization. Cryosph. 9, 179–196 doi: 10.5194/tc-9-179-2015 (2015).

[16] Siddall, M. *et al*. Sea-level fluctuations during the last glacial cycle. *Nature* **423**, 853–858, doi:10.1038/nature01690 (2003).

[17] Rohling, E. J. *et al*. Antarctic temperature and global sea level closely coupled over the past five glacial cycles. *Nature Geosci.* **2**, 500–504, doi:10.1038/ngeo557 (2009).

[18] Grant, K. M. *et al*. Sea-level variability over five glacial cycles. *Nature Comm.* **5**, doi:10.1038/ncomms6076 (2014).

[19] Marino, G. *et al*. Bipolar seesaw control on last interglacial sea level. *Nature* **522**, 197–201, doi:10.1038/nature14499 (2015).

[20] Barlow, N. L. *et al*. Lack of evidence for a substantial sea-level fluctuation within the Last Interglacial. *Nature Geosci.* **11**, 627–634, doi: 10.1038/s41561-018-0195-4 (2018).

[21] Overpeck, J. T. *et al*. Paleoclimatic evidence for future ice-sheet instability and rapid sea-level rise. *Science* **311**, 1747–1750, doi:10.1126/science.1115159 (2006).

[22] Vyverberg, K. *et al*. Episodic reef growth in the granitic Seychelles during the Last Interglacial: implications for polar ice sheet dynamics. *Mar. Geol.* **399,** 170–187, doi:10.1016/j.margeo.2018.02.010 (2018).

[23] Thompson, W. G., Curran, H. A., Wilson, M. A. & White, B. Sea-level oscillations during the last interglacial highstand recorded by Bahamas corals. *Nature Geosci.* **4,** 684–687, doi:10.1038/NGEO1253 (2011).

[24] Moseley, G. E., Smart, P. L., Richards, D. A. & Hoffmann, D. L. Speleothem constraints on marine isotope stage (MIS) 5 relative sea levels, Yucatan Peninsula, Mexico. *J. Quat. Sci.* **28,** 293–300 doi: 10.1002/jqs.2613 (2013).

[25] Long, A. J. *et al*. Near-field sea-level variability in northwest Europe and ice sheet stability during the last interglacial. *Quat. Sci. Rev.* **126**, 26–40, doi:10.1016/j.quascirev.2015.08.021 (2015).

[26] Cutler, K. B. *et al*. Rapid sea-level fall and deep-ocean temperature change since the last interglacial period. *Earth Planet. Sci. Lett.* **206,** 253–271 doi: 10.1016/S0012-821X(02)01107-X (2003).

[27] Tzedakis, P.C. *et al*. Enhanced climate instability in the North Atlantic and southern Europe during the Last Interglacial. *Nature Comm.* **9**, doi: 10.1038/s41467-018-06683-3 (2018).

[28] Deaney, E. L., Barker, S. & van de Flierdt, T. Timing and nature of AMOC recovery across Termination 2 and magnitude of deglacial CO_2 change. *Nature Comm.* **8**, doi:10.1038/ncomms14595 (2017).

[29] Siddall, M. *et al*. Understanding the Red Sea response to sea level. *Earth Planet. Sci. Lett.* **225**, 421–434, doi:10.1016/j.epsl.2004.06.008 (2004).

[30] Plaziat, J. -C., Reyss, J. -L., Choukri, A. & Cazala, C. Diagenetic rejuvenation of raised coral reefs and precision of dating. The contribution of the Red Sea reefs to the question of reliability of the Uranium-series datings of middle to late Pleistocene key reef-terraces of the world. *Carnets Géologie / Notebooks Geology* **4,** 2008/04 (2008).

[31] Orszag-Sperber, F., Plaziat, J. C., Baltzer, F. & Purser, B. H. Gypsum salina-coral reef relationships during the Last Interglacial (Marine Isotopic Stage 5e) on the Egyptian Red Sea coast: a Quaternary analogue for Neogene marginal evaporites? *Sediment. Geol.* **140**, 61–85 doi: 10.1016/S0037-0738(00)00172-X (2001).

[32] Bruggemann, J. H. *et al*. Stratigraphy, palaeoenvironments and model for the deposition of the Abdur Reef Limestone: context for an important archaeological site from the last interglacial on the Red Sea coast of Eritrea. *Palaeogeogr. Palaeoclimatol. Palaeoecol.* **203**, 179–206 doi: 10.1016/S0031-0182(03)00659-X (2004).

[33] Hellmer, H. H., Kauker, F., Timmermann, R., Determann, J. & Rae, J. Twenty-first-century warming of a large Antarctic ice-shelf cavity by a redirected coastal current. *Nature* **485,** 225–228 doi: 10.1038/nature11064 (2012).

[34] Fogwill, C. J., Phipps, S. J., Turney, C. S. M. & Golledge, N. R. Sensitivity of the Southern Ocean to enhanced regional Antarctic ice sheet meltwater input. *Earth's Future* **3**, 317–329 doi: 10.1002/2015EF000306 (2015).

[35] Phipps, S. J., Fogwill, C. J. & Turney, C. S. M. Impacts of marine instability across the East Antarctic Ice Sheet on Southern Ocean dynamics. *The Cryosphere* **10**, 2317–2328 doi: 10.5194/tc-10-2317-2016 (2016).

[36] Hayes, C. T. *et al*. A stagnation event in the deep South Atlantic during the last interglacial period. *Science* **346**, 1514–1517, doi:10.1126/science.1256620 (2014).

[37] Adkins, J. F. The role of deep ocean circulation in setting glacial climates. *Paleoceanography* **28,** 539–561 doi: 10.1002/palo.20046 (2013).

[38] Ninnemann, U. S., Charles, C. D. & Hodell, D. A. Origin of Global Millennial Scale Climate Events: constraints from the Southern Ocean deep sea sedimentary record. in *Geophysical Monograph Series volume 112, Mechanisms of Global Climate Change at Millennial Time Scales* (eds. Clark, P. U., Webb, R. S. & Keigwin, L. D.) 99–112 (American Geophysical Union, 1999). doi:10.1029/GM112p0099.

[39] Silvano, A. *et al.* Freshening by glacial meltwater enhances melting of ice shelves and reduces formation of Antarctic Bottom Water. *Sci. Adv.* **4,** eaap9467 doi: 10.1126/sciadv.aap9467 (2018).

[40] Vaughan, D. G., Barnes, D. K. A., Fretwell, P. T. & Bingham, R. G. Potential seaways across West Antarctica. *Geochemistry, Geophys. Geosystems* **12**, Q10004 doi: 10.1029/2011GC003688 (2011).

597 [41] Holden, P. B. *et al.* Interhemispheric coupling, the West Antarctic Ice Sheet and
598 warm Antarctic interglacials. *Clim. Past* **6**, 431–443 doi: 10.5194/cp-6-431-
599 2010 (2010).
600 [42] Steig, E. J. *et al.* Influence of West Antarctic Ice Sheet collapse on Antarctic
601 surface climate. *Geophys. Res. Lett.* **42**, 4862–4868 doi:
602 10.1002/2015GL063861 (2015).
603 [43] Holloway, M. D. *et al.* Antarctic last interglacial isotope peak in response to sea
604 ice retreat not ice-sheet collapse. *Nat. Commun.* **7**, 12293
605 doi: 10.1038/nature10902 (2016).
606 [44] Gomez, N., Mitrovica, J. X., Tamisiea, M. E. & Clark, P. U. A new projection of sea
607 level change in response to collapse of marine sectors of the Antarctic Ice
608 Sheet. *Geophys. J. Int.* **180**, 623–634, doi:10.1111/j.1365-246X.2009.04419.x
609 (2010).
610 [45] Gomez, N., Pollard, D. & Mitrovica, J. X. A 3-D coupled ice sheet – sea level
611 model applied to Antarctica through the last 40 ky. *Earth Planet. Sci. Lett.* **384**,
612 88–99 doi: 10.1016/j.epsl.2013.09.042 (2013).
613 [46] Gomez, N., Pollard, D. & Holland, D. Sea-level feedback lowers projections of
614 future Antarctic Ice-Sheet mass loss. *Nat. Commun.* **6**, 8798
615 doi: 10.1038/ncomms9798 (2015).
616 [47] Konrad, H., Sasgen, I., Pollard, D. & Klemann, V. Potential of the solid-Earth
617 response for limiting long-term West Antarctic Ice Sheet retreat in a warming
618 climate. *Earth Planet. Sci. Lett.* **432**, 254–264, doi:10.1016/j.epsl.2015.10.008
619 (2015).
620 [48] Bradley, S. L., Hindmarsh, R. C. A., Whitehouse, P. L., Bentley, M. J. & King, M. A.
621 Low post-glacial rebound rates in the Weddell Sea due to Late Holocene ice-
622 sheet readvance. *Earth Planet. Sci. Lett.* **413**, 79–89 doi:
623 10.1016/j.epsl.2014.12.039 (2015).
624 [49] Kingslake, J. *et al.* Extensive retreat and re-advance of the West Antarctic Ice
625 Sheet during the Holocene. *Nature* **558**, 430–434 doi: 10.1038/s41586-018-
626 0208-x (2018).
627 [50] Wolff, E. W. *et al.* Changes in environment over the last 800,000 years from
628 chemical analysis of the EPICA Dome C ice core. *Quat. Sci. Rev.* **29**, 285–295
629 doi: 10.1016/j.quascirev.2009.06.013 (2010).

[51] DeConto, R. M. & Pollard, D. Contribution of Antarctica to past and future sea-level rise. *Nature* **531**, 591–597, doi:10.1038/nature17145 (2016).

[52] Menviel, L., Timmermann, A., Timm, O. E. & Mouchet, A. Climate and biogeochemical response to a rapid melting of the West Antarctic Ice Sheet during interglacials and implications for future climate. *Paleoceanography* **25**, doi:10.1029/2009pa001892 (2010).

[53] Rignot, E., Mouginot, J., Morlighem, M., Seroussi, H. & Scheuchl, B. Widespread, rapid grounding line retreat of Pine Island, Thwaites, Smith, and Kohler glaciers, West Antarctica, from 1992 to 2011. *Geophys. Res. Lett.* **41**, 3502–3509, doi:10.1002/2014gl060140 (2014).

[54] Golledge, N. R. *et al*. The multi-millennial Antarctic commitment to future sea-level rise. *Nature* **526**, 421–425, doi:10.1038/nature15706 (2015).

[55] Jenkins, A. *et al*. Decadal ocean forcing and Antarctic Ice Sheet response: lessons from the Amundsen Sea. *Oceanography* **29**, 106–117, doi:10.5670/oceanog.2016.103 (2016).

[56] The IMBIE team. Mass balance of the Antarctic Ice Sheet from 1992 to 2017. *Nature* **558**, 219–222, doi:10.1038/s41586-018-0179-y (2018).

[57] King, M. D. *et al.* Seasonal to decadal variability in ice discharge from the Greenland Ice Sheet. *Cryosphere* **12**, 3813–3825 doi: 10.5194/tc-12-3813-2018 (2018).

[58] van den Broeke, M. R. *et al.* On the recent contribution of the Greenland ice sheet to sea level change. *Cryosphere* **10**, 1933–1946 doi: 10.5194/tc-10-1933-2016 (2016).

[59] Rohling, E. J. *et al.* Magnitudes of sea-level lowstands of the past 500,000 years. *Nature* **394**, 162–165 doi: 10.5194/cp-7-941-2011 (1998).

[60] Fenton, M. *Late Quaternary history of Red Sea outflow.* PhD Thesis Southampton University (1998).

[61] Sambridge, M. Reconstructing time series and their uncertainty from observations with universal noise. *J. Geophys. Res.: Solid Earth* **121**, 4990–5012, doi:10.1002/2016JB012901 (2016).

[62] Shackleton, N. J. Attainment of isotopic equilibrium between ocean water and the benthonic foraminifera genus *Uvigerin*a: isotopic changes in the ocean

during the last glacial. *Colloq. Int. Centre Natl Rech. Scient.* **219**, 203–210 (1974).

[63] Irvali, N. *et al.* Rapid switches in subpolar North Atlantic hydrography and climate during the Last Interglacial (MIS 5e). *Paleoceanography* **27**, doi:10.1029/2011pa002244 (2012).

[64] Irvali, N. *et al*. Evidence for regional cooling, frontal advances, and East Greenland Ice Sheet changes during the demise of the last interglacial. *Quat. Sci. Rev.* **150**, 184–199, doi:10.1016/j.quascirev.2016.08.029 (2016).

[65] Bazin, L. *et al.* An optimized multi-proxy, multi-site Antarctic ice and gas orbital chronology (AICC2012): 120-800 ka. *Clim. Past* **9,** 1715–1731 doi: 10.5194/cp-9-1715-2013 (2013).

[66] Cox, K. A. *et al*. Interannual variability of Arctic sea ice export into the East Greenland Current. *J. Geophys. Res.: Oceans* **115**, doi:10.1029/2010jc006227 (2010).

[67] Stanford, J. D., Rohling, E. J., Bacon, S. & Holiday, N. P. A review of the deep and surface currents around Eirik Drift, south of Greenland: comparison of the past with the present. *Global Planet. Change* **79**, 244–254, doi:10.1016/j.gloplacha.2011.02.001 (2011).

[68] Jouzel, J. *et al*. Orbital and millennial Antarctic climate variability over the past 800,000 years. *Science* **317**, 793–796, doi:10.1126/science.1141038 (2007).

[69] Martrat, B., Jimenez-Amat, P., Zahn, R. & Grimalt, J. O. Similarities and dissimilarities between the last two deglaciations and interglaciations in the North Atlantic region. *Quat. Sci. Rev.* **99**, 122–134, doi:10.1016/j.quascirev.2014.06.016 (2014).

[70] Bereiter, B. *et al.* Revision of the EPICA Dome C CO_2 record from 800 to 600 kyr before present. *Geophys. Res. Lett.* **42,** 542–549 doi: 10.1002/2014GL061957 (2015).

[71] Wolff, E. W. *et al.* Southern Ocean sea-ice extent, productivity and iron flux over the past eight glacial cycles. *Nature* **440,** 491–496 doi: 10.1038/nature04614 (2006).

[72] Petit, J. R. *et al.* Climate and atmospheric history of the past 420,000 years from the Vostok ice core, Antarctica. *Nature* **399,** 429–436 doi: 10.1038/20859 (1999).

[73] Galaasen, E. V. *et al.* Rapid reductions in North Atlantic Deep Water during the peak of the Last Interglacial period. *Science* **343,** 1129–1132 doi: 10.1126/science.1248667 (2014).

Author contributions. EJR and FDH led the research. KMG, GM, FW, and JY added wider documentation and context. HS contributed core curation, sampling, and processing assistance. EVG, NI, KK, UN, and YR provided new oxygen isotope and microfossil shell chemistry records for Eirik Drift. APR helped shape the initial concept and focussed the presentation. All co-authors assisted in producing the manuscript.

Competing interests. The authors declare no competing interests.

Acknowledgements. This research contributes to Australian Research Council Laureate Fellowship FL120100050 (EJR). UiB contribution (EVG, Ni, KK and UN) supported by RCN project THRESHOLDS (25496). GM acknowledges generous support from the University of Vigo. All plotted new data will be made openly available via http://www.highstand.org/erohling/ejrhome.htm.

Figure 1. Global summary of stratigraphic evidence for Last Interglacial sea-level instability in coral-reef deposits and coastal-sediment sequences. Blue dot is the location of Hanish Sill, the constraining point for the Red Sea sea-level record. Red squares with white centers are stratigraphically superimposed coral reef or sedimentary archives for sea-level oscillations within the Last Interglacial (LIG). Solid red dots are locations where sea-level oscillations are inferred but where there is no stratigraphic superposition. The underlying map is of the difference between maximum Last Interglacial (LIG) relative sea level (RSL) values for glacio-isostatic adjustment (GIA) modelling results based on two contrasting ice models (ICE-1 and ICE-3) for the penultimate glaciation using Earth model E1 (VM1-like set up). The ICE-1 model is a version of the ICE-5G ice history (LGM-like), whereas ICE-3 has both reduced total ice volume relative to ICE-1, and a different ice-mass distribution (i.e., a smaller North American Ice Sheet complex and larger Eurasian Ice Sheet) that is consistent with glaciological reconstructions of the penultimate glacial period[4].

Figure 2. Variability in Last Interglacial sea-level time-series. Yellow bar: time-interval of Heinrich Stadial 11 (HS11)[19]. Orange bar: approximate interval of temporary sea-level drop in various records. Dashed line: end of main LIG highstand set to 118.5 ka (cross-bar indicates 95% confidence limits of ±1.2 ka), based on compilations in (**b**) and the speleothem sea-level "ceiling" (**c**). **a.** GrIS contributions to sea level from a model-based assessment of Greenland ice-core data (blue)[9], and changes in surface sea-water $\delta^{18}O$ at Eirik Drift (black; this study) with uncertainties (2σ) determined from underpinning $\delta^{18}O$ and Mg/Ca measurement uncertainties and Mg/Ca calibration uncertainties. **b.** 95% probability interval for coral sea-level markers above 0 m[11] (brown), and LIG duration from a previous compilation (black)[26]. **c.** Red Sea RSL stack (red, including KL23) with 1σ error bars. Smoothings are shown to highlight general trends only, and represent simple polynomial regressions with 68% and 95% confidence limits (orange shading and black dashes, respectively). Purple line indicates the sea-level "ceiling" indicated by subaerial speleothem growth (Yucatan)[24]. **d.** Probability maximum (PM, lines) and its 95% confidence interval for Antarctic temperature changes (red)[68], and proxy for eastern

Atlantic water temperature (ODP976, grey)[69]. Blue crosses: composite record of atmospheric CO_2 concentrations from Antarctic ice cores[19]. **e.** Individual records for Red Sea cores KL11 (blue, dots) and KL23 (red, plusses), with 300-year moving Gaussian smoothings (as used in Ref.1). Also shown is a replication exercise to validate the single-sample earliest-LIG peak in KL23 (grey, filled squares) with 1 standard error intervals (bars, $\sigma/\sqrt{\{N\}}$, based on N= 5, 5, 4, 4, and 5 replications, from youngest to oldest sample, respectively). Separate blue cross indicates typical uncertainties (1σ) in individual KL11 data points prior to probabilistic analysis of the record. **f.** Probabilistic analysis of the KL11 Red Sea RSL record, taking into account the strict stratigraphic coherence of this record. Results are reported for the median (50th percentile, dashed yellow), PM (modal value, black), the 95% probability interval of the PM (dark grey shading), and both the 68% and 95% probability intervals for individual datapoints (intermediate and light grey shading, respectively).

Figure 3. Identification of Greenland Ice Sheet and Antarctic Ice Sheet contributions to Last Interglacial sea-level variations. a. Global Mean Sea Level (GMSL) approximation based on the probabilistically assessed KL11 PM (black line) and its 95% probability interval (grey). This record is shown in terms of RSL in Figure 2f, but here includes the glacio-isostatic correction and its propagated uncertainty. Black triangles identify limits between sea-level rises R1, R2, and R3 were measured. Rates of rise with 95% bounds: R1 = 2.8 (1.2-3.7) m c^{-1}; R2 = 2.3 (0.9-3.5) m c^{-1}; R3 = 0.6 (0.1-1.3) m c^{-1}. **b.** Blue: GrIS sea-level contribution from the model-data assimilation of Ref. [9] (shading represents the 95% probability interval). Grey: GrIS contribution based on Eirik Drift $\delta^{18}O_{sw}$. Uncertainties as in Figure 2a. Orange: AIS contribution from subtraction of the blue GrIS reconstruction from the record in (**a**). Green: AIS contribution found by subtracting the grey GrIS reconstruction from the record in (**a**). Orange and green AIS reconstructions are shown as medians (lines) and 95% confidence intervals (shading). Reconstructed AIS contributions cross downward through a fine dashed when they fall below –10 m, which indicates a rough maximum AIS growth limit in terms of sea-level lowering (AIS growth is limited by Antarctic

783 continental shelf edges). When the green/orange curves fall below these limits,
784 North American and/or Eurasian ice-sheet growth is likely implied. The key
785 result from the present study lies in identification of GrIS and AIS sea-level
786 contributions above 0 m. **c.** Southern Ocean ODP (Ocean Drilling Program) Site
787 1094 authigenic uranium mass accumulation rates, on its original, Antarctic Ice
788 Core Chronology (AICC2012) tuned, age model. Dashed lines indicate potential
789 offsets (within uncertainties) between the ODP 1094 AICC2012-based
790 chronology[36] and our LIG chronology[10,19, this study].
791
792
793 **Figure 4. Timing of Antarctic Ice Sheet retreat relative to circum-Antarctic**
794 **climate and ocean warming.** LIG records of **a.** Antarctic ice core composite
795 atmospheric CO_2[70], **b.** EPICA Dome C sea-salt Na flux (on a logarithmic scale),
796 which reflects Southern Ocean sea-ice extent[71], **c.** Vostok δD (lilac)[65,72], **d.** Site
797 1089 planktic foraminiferal (*G. bulloides*) $\delta^{18}O$ (red)[38], **e.** Site 1094 TEX_{86}^{L}-based
798 sea surface temperatures (orange)[36], **f.** Site 1089 planktic minus benthic
799 foraminiferal $\delta^{18}O$ (‰) plotted as 3-point running mean (red) and sample
800 average including combined 1-sigma uncertainty (light red shading)[38], **g.** Site
801 1094 authigenic uranium (aU) accumulation where higher values indicate
802 bottom water deoxygenation[36], **h.** Site 1063 ε_{Nd} (dark blue, measured by MC-
803 ICP-MS; light blue, measured by TIMS)[28], and **i.** bottom water $\delta^{13}C$ records from
804 Site 1063 (blue, 3-point running mean, based on benthic foraminifera
805 *Cibicidoides wuellerstorfi*, *Melonis pompilioides*, and *Oridorsalis*)[28], MD03-2664
806 (yellow, 3-point running mean, *C. wuellerstorfi*)[73], Site 1089 (red, *C.*
807 *wuellerstorfi*)[36], and Site 1094 (orange, *C. wuellerstorfi*)[36]. **g.** and **h.** indicate
808 North Atlantic Deep Water (NADW) influence as denoted. Map inset includes
809 marine core locations, plotted using Ocean Data View (https://odv.awi.de).
810
811
812
813
814
815

Figure 1.

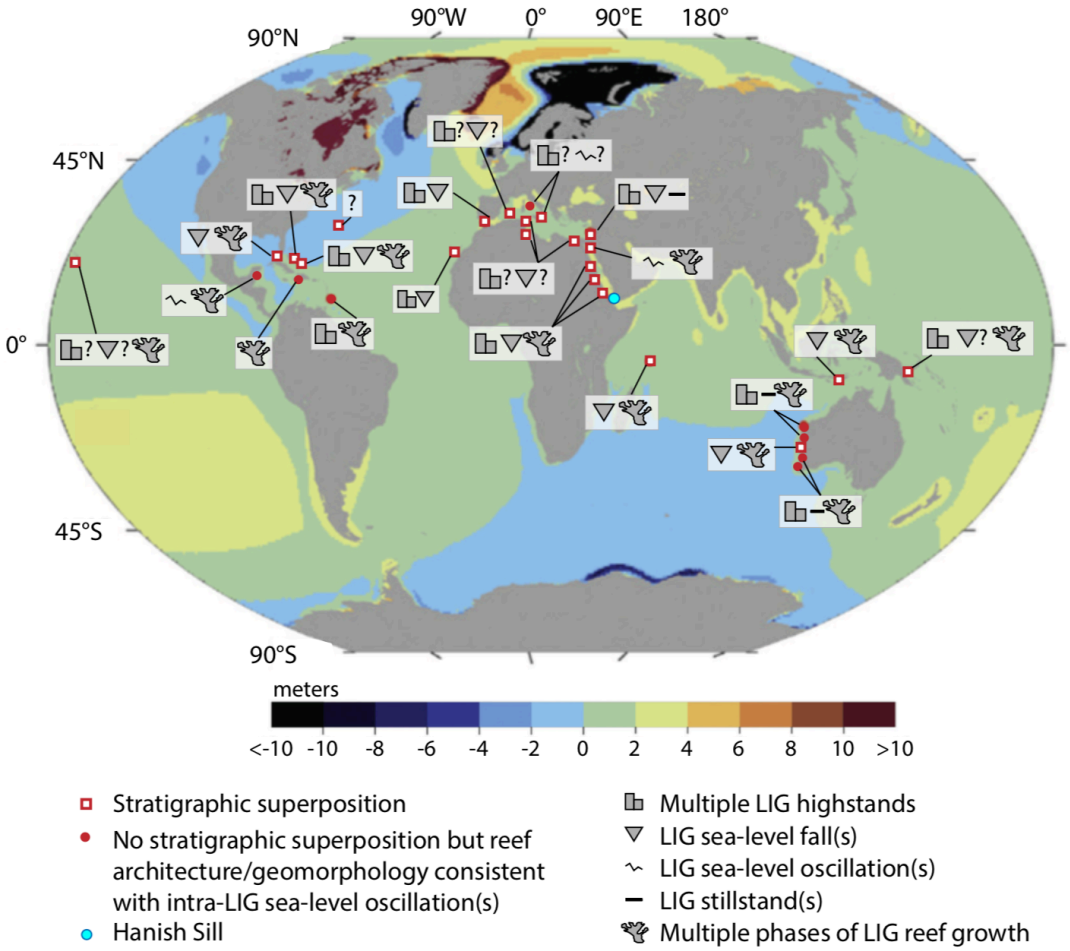
90°W
0°
90°E
180°
90°N
45°N
0°
45°S
90°S
meters
<-10 -10 -8 -6 -4 -2 0 2 4 6 8 10 >10
Stratigraphic superposition
No stratigraphic superposition but reef architecture/geomorphology consistent with intra-LIG sea-level oscillation(s)
Hanish Sill
Multiple LIG highstands
LIG sea-level fall(s)
LIG sea-level oscillation(s)
LIG stillstand(s)
Multiple phases of LIG reef growth

Figure 2.

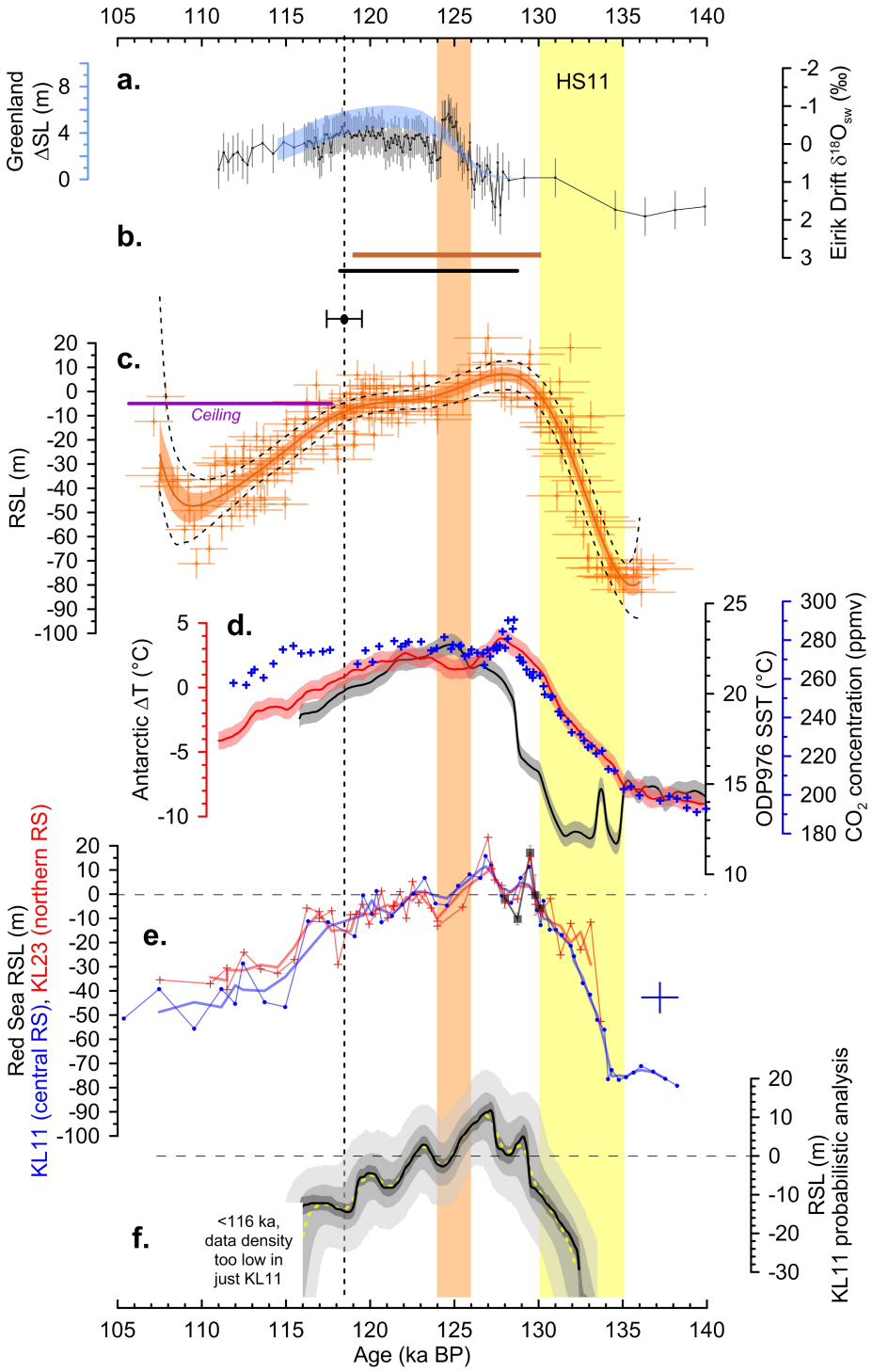
105
110
115
120
125
130
135
140
a.
HS11
Greenland ΔSL (m)
8
4
0
-2
-1
0
1
2
3
Eirik Drift $\delta^{18}O_{sw}$ (‰)
b.
c.
Ceiling
RSL (m)
20
10
0
-10
-20
-30
-40
-50
-60
-70
-80
-90
-100
d.
Antarctic ΔT (°C)
5
0
-5
-10
25
20
15
10
ODP976 SST (°C)
300
280
260
240
220
200
180
CO_2 concentration (ppmv)
e.
Red Sea RSL (m)
KL11 (central RS), KL23 (northern RS)
f.
<116 ka,
data density
too low in
just KL11
KL11 probabilistic analysis
RSL (m)
Age (ka BP)

Figure 3

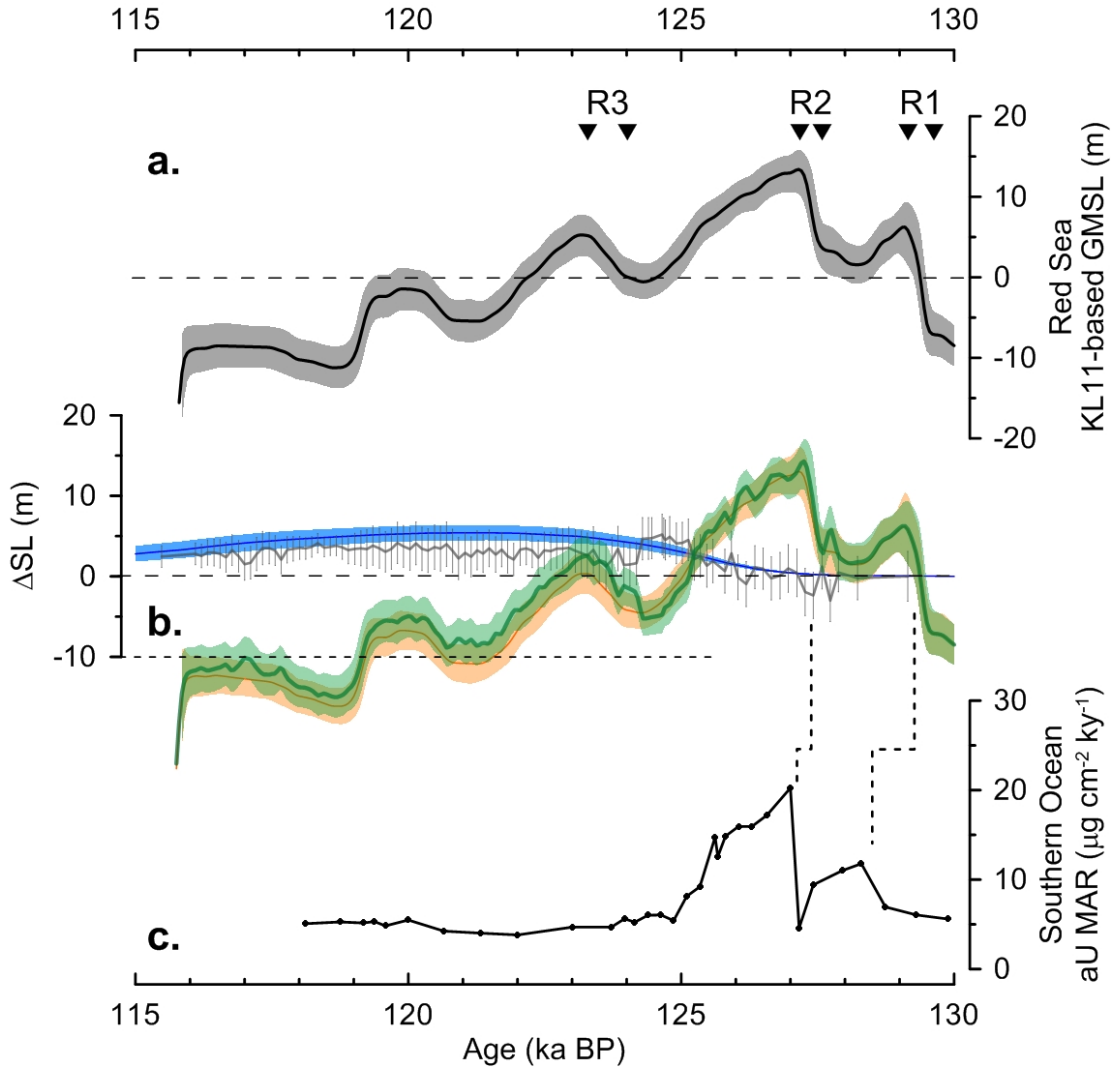
115
120
125
130
R3
R2
R1
a.
20
10
0
-10
-20
Red Sea
KL11-based GMSL (m)
ΔSL (m)
20
10
0
-10
b.
c.
30
20
10
0
Southern Ocean
aU MAR (μg cm-2 ky-1)
115
120
125
130
Age (ka BP)

Figure 4.

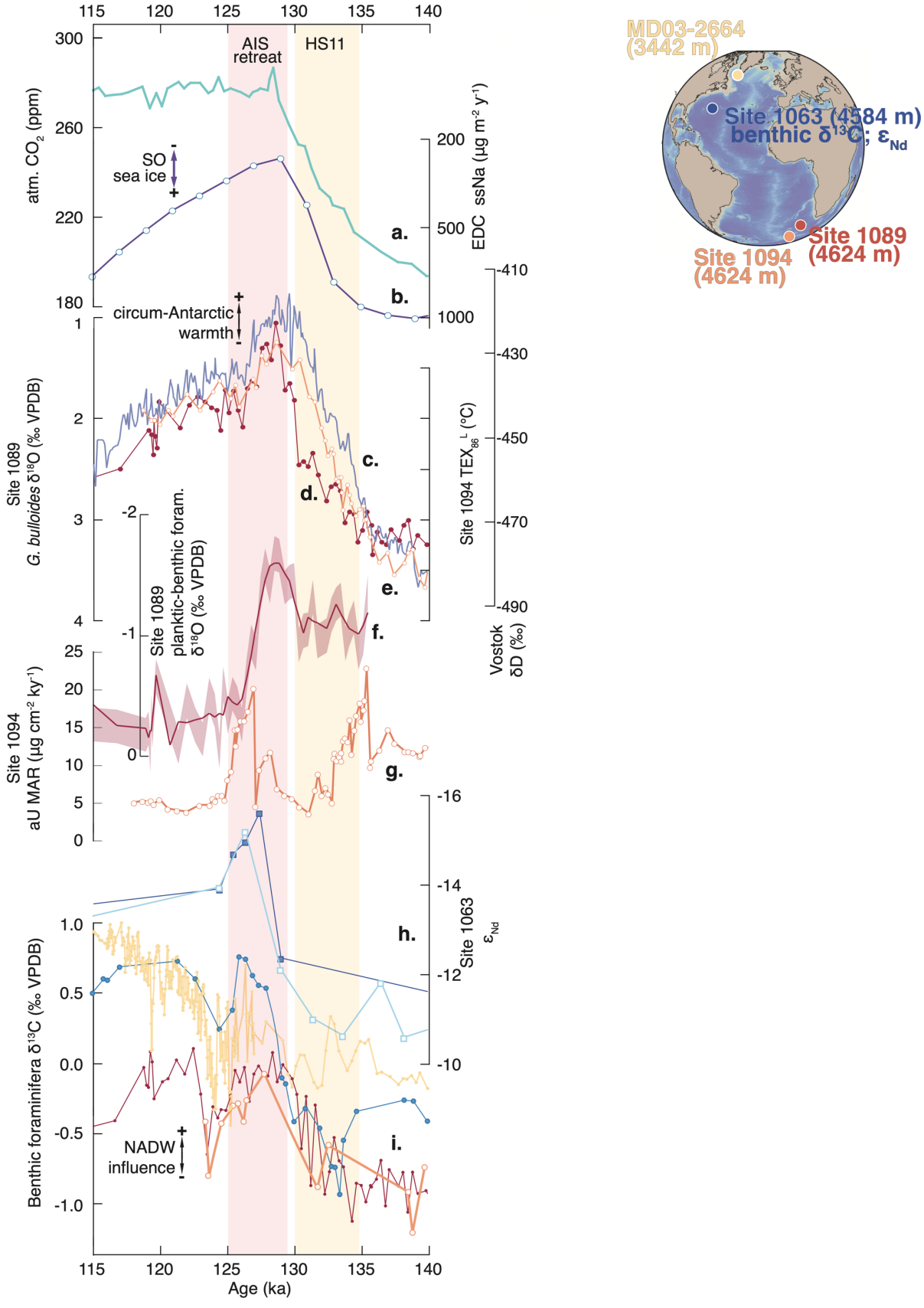
AIS retreat
HS11
atm. CO2 (ppm)
SO sea ice
EDC ssNa (µg m-2 y-1)
a.
b.
circum-Antarctic warmth
Site 1089 G. bulloides δ18O (‰ VPDB)
Site 1094 TEXL86 (°C)
c.
d.
Site 1089 planktic-benthic foram. δ18O (‰ VPDB)
e.
f.
Vostok δD (‰)
Site 1094 aU MAR (µg cm-2 ky-1)
g.
Site 1063 εNd
h.
Benthic foraminifera δ13C (‰ VPDB)
NADW influence
i.
Age (ka)
MD03-2664 (3442 m)
Site 1063 (4584 m) benthic δ13C; εNd
Site 1089 (4624 m)
Site 1094 (4624 m)

Supplementary Information:

Asynchronous Antarctic and Greenland ice-volume contributions to the last interglacial sea-level highstand

Rohling et al.

Supplementary Note 1.

Stratigraphic evidence of Last Interglacial sea-level instability

The following is a discussion of selected Last Interglacial (LIG) sites that contain stratigraphically coherent records of sea-level oscillations, mostly from far-field locations (*Supplementary Figure* 1). We first discuss sites with stratigraphic superposition (section 1A), followed by sites with reef architecture or geomorphology consistent with intra-LIG sea-level oscillation(s) but where sediments or reef units do not overlie one another directly (section 1B) (for a map of sites discussed, see *Supplementary Figure* 1).

This is intended as an overview (rather than an exhaustive review) of the extensive literature on LIG sea levels. There is much divergence among records, but we provide a short synthesis (section 1C) that portrays an emerging picture of LIG sea levels from coral reef evidence. We report facies and stratigraphic interpretations, and ages as reported in the original publications. In addition, the sea-level archive and key features of the record are given in square brackets, where key features are: mH = multiple LIG sea-level highstands; Fall = inter-LIG sea-level fall(s); Stillstand = LIG sea-level stillstand(s); oscillation = oscillations in LIG sea levels; mPG = multiple phases of LIG reef growth; ? = evidence uncertain or debated.

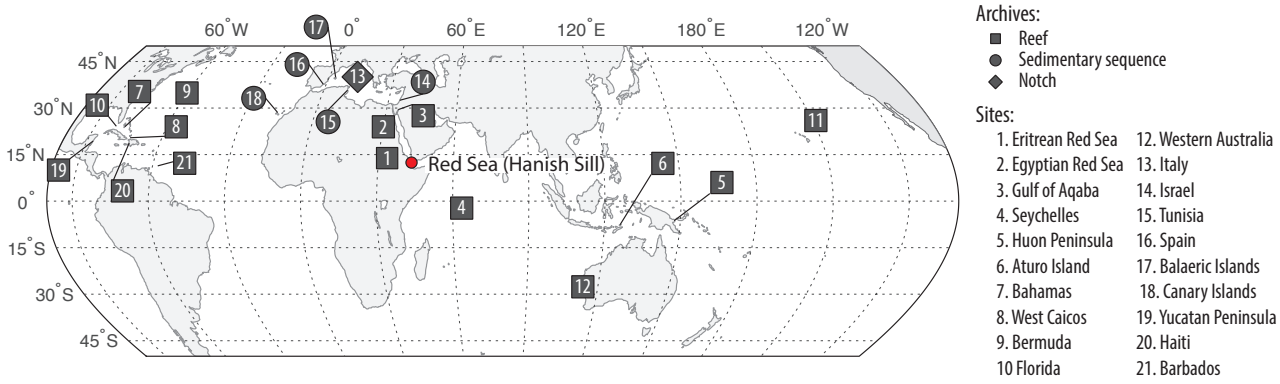

Supplementary Figure 1. Global summary of stratigraphic evidence for Last Interglacial sea-level instability in coral-reef deposits and coastal-sediment sequences. Red dot is the location of the Red Sea sea-level record.

(1A) CONSTRUCTIONAL REEF OR SEDIMENTARY SEQUENCES

1. Red Sea

1.1. Eritrean Red Sea coast [reef; mH, Fall & mPG]:

The Abdur Reef Limestone complex is a MIS 5e marine terrace sequence that contains two superimposed stages of shallow reef development[1,2]. The lower unit is truncated by an intermittent marine erosion surface, which is directly overlain by reef-crest/reef-front coral assemblages. The erosional surfaces that separatethe marine subunits are interpreted as periods of interrupted sedimentation and reef growth[2]. The complete LIG sequence is: a basal lag deposit overlain by grainstone or floatstone facies, which fines upward to suggest rapid deepening. This was followed by shoaling and development of a local reef and the coral proliferation. The top of this marine subunit is a hardground/erosional surface with submarine lithification, and with biological reworking evident. This is inferred to have occurred when the surface was at intertidal depths, during or slightly after the sea-level lowering (the authors are uncertain if the hardground ever emerged). The erosional surface

is overlain by extensive coral reef growth and the typical corals exposed suggest that this is a reef flat in growth position (the authors suggest that this platform rim was near sea level). This reef unit is overlain by reef subunit $5e_3$ with encrusting oysters on the surface that may indicate an additional sea-level lowering or still stand. A subsequent sea level rise is indicated by patches of *in situ* corals that overlie this reef unit[2]. Precise age control for these reefs is difficult; all current U-series dates[1] do not meet commonly accepted age 'reliability' criteria.

1.2 Egyptian coast, Red Sea: [reef; mH Fall & mPG]:
A continuous coastal reef and beach unit extends along nearly 500 km of the Egyptian Red Sea coast[3]. Three distinct sea-level oscillations are suggested for the LIG: (1) a compound first phase with (*1.1*) an initial highstand (elevations ~+6 to +8 m) and (*1.2*) a subsequent (brief) transgression (~+3 m above the previous highstand) - note, this second phase is seen only at the protected sites of Sharm el Naga and Sharm el Bahari, which suggests limited reef growth during this second phase; (2) a short-lived lowstand (with a sea-level drop of up to 10 m[Ref.4,5]; and (3) a subsequent (final) sea-level rise (~+6 m elevation). U-series ages for corals in this region are often affected by diagenesis and open system behaviour. Plaziat et al. (1998)[Ref.4] derive ages for LIG sea-level events by correlating with the global $\delta^{18}O$ stack of Pisias et al. (1984) rather than by direct dating.

1.3 Gulf of Aqaba: [reef; oscillation; mPG]
A flight of coral terraces (on an uplifting coastline) offers potential age constraints for the Red Sea LIG coral record. The superimposed reefs are evidence for sea-level oscillations, with one and possibly two stillstands, during the last interglacial. The three coral units are dated at the "Bedouin Village" site[6,7]. The highest terrace (R3) has limited expression and altered ages (elevation +20 m apsl) but suggests an "earliest part of the MIS 5e highstand around 132-130 ka". The second LIG terrace (R2) (elevation +12 to +18 m apsl) is found a couple of metres below R3 in elevation with sea levels inferred to be +5 m apsl[6]. It should be noted that the corals have been altered extensively to calcite (evident in most corals in the R2, R3 and R4 terraces), which complicates dating of these corals. Ages for these sites are calculated assuming recrystallization during a single period of open-system behaviour that lasted a few hundred years, followed by closed-system behaviour[7].

2. Seychelles: [reef**;** FALL, mPG]
The Seychelles record[8–10] contains evidence of multiple (superimposed) LIG reef growth generations, with at least one short-lived ("ephemeral") sea-level fall/stillstand (evident as distinct lithological and assemblage changes/coral rubble layer). Exposures of patchy veneers of marine limestones that adhere to granitic boulders in an area protected from weathering contain exhibit a conglomerate/rubble layer intercalated between coral units[8–10]. There appear to be "at least three distinct reef-growth episodes punctuated by two discontinuities that typically manifest as coral rubble layers or extensive encrustations of the hydrozoan coral *Millepora exaesa*"[9,10]. At two sites, extensive dissolution and freshwater cements are associated with the disturbance layers, which suggest sub-aerial exposure followed by marine inundation[10]. U-series ages for the rubble deposition event between the first and second episodes of reef growth are regionally consistent between two islands at ~126-125 ka[Ref.9] and "may reflect ephemeral sea-level fall"[Ref.10]. Further, "field evidence and dating from high marine limestones from two sections at La Digue Island indicate a period of coral buildup until 131,000 yr B.P., followed by a drop in sea level between 131,000 and 122,000 yr B.P." (Israelson and Wolfarth, 1999). However, "…only two corals from the

Israelson and Wohlfarth (1999) study pass the screening criteria (Fig. 7a): these two corals have identical ages (123.8 ± 0.5 ka) and occur at an elevation near +4 m. These two samples (90/1 and 90/2) are described as being capped by coralgal-vermetid layers (Israelson and Wohlfarth, 1999), and if they grew up to the intertidal zone may represent a drop in sea level from the +6.6 ± 0.2 m attained at 125.1 ± 0.4 ka."[Ref.9]. Dutton et al. (2015)[Ref.9] could not replicate/corroborate this "tentative" interpretation because the outcrop had subsequently weathered away. However, the most recent study by Vyverberg et al. (2018)[Ref.10] confirms "clear evidence of multiple interruptions in reef growth where well-developed reef units are separated by disturbance… Our observations are consistent with prior suggestions that the LIG sea level highstand was characterized by multiple peaks in sea level". Ages for the two reef-growth episodes described by Vyverberg et al. (2018)[Ref.10] are not yet published. Israelson and Wolfarth (1999)[Ref.8] suggested a magnitude of any sea level fall of ~2 m but, given that reefs are primarily constructional features, this estimate may not fully capture the full range of any sea level fall.

3. Huon Peninsula, Papua New Guinea: [reef; mH, Fall?, mPG]
The Huon Peninsula has an extensive (laterally more than 80 km[Ref.11]) flight of uplifted terraces. The LIG reef VII complex consists of a barrier reef (VIIb), a lagoon, and a fringing reef (VIIa), which has led some to suggest the possibility of two phases of rapid sea-level rise[11–13]. A significant sea-level oscillation is inferred between VIIb and VIIa, based on reef-growth interruption beneath the VIIb barrier (marked by a visible sloping surface in one exposure, with no coral growth crossing the surface[11,12]. Aharon et al. (1980)[Ref.14] described this as an erosional disconformity, associated with a "minor" sea-level fall following an initial sea-level rise and a subsequent < 8 m rise "during the building of VIIb crest"[14]. However, a subsequent expedition in 1988 found no distinctive subaerial features associated with this inferred reef cessation/sea level fall[13]. U-series ages[13] for these two reef units fall into two distinct groups; reef unit VIIb ages cluster at about 118 and 143 ka, and VIIa corals (~3 m below crest of VIIb) centre at about ~118 ka. The apparent lack of corals with intermediate ages led Stein et al. (1993)[Ref.13] to suggest two episodes of LIG sea-level rise, despite significant diagenetic alteration (recrystallization from aragonite to calcite) of corals.

4. Atauro Island: [reef; FALL, mPG]
Atauro Island (north of East Timor/Timor-Leste) has an inter-fingering sequence of reef units, with Reef 2 corresponding to the LIG and an unconformity separating two LIG transgressive subunits[11,12]. In general, three units are recognised in reef 2; reef 2 main (the main body of the reef) overlies an older reef (reef 2-lower); reef 2-main is capped by cobble pavement, which is in turn overlain by a shallow water reef. An additional reef 2-late is recognised in one location and is a small reef remnant beneath a cliff cut into reef 2[Ref.12]. This sequence is interpreted as an initial episode of reef building, followed by a sea-level fall and a subsequent reef-growth episode (reef 2-main). Reef 2-main was possibly interrupted (given the gravels separating reef 2-main and reef 2-upper), although this may have been due to continued tectonic uplift rather than a sea-level change. A major sea-level lowering event (~27 m) may have been interrupted by minor sea-level rise and growth of reef 2-late[Ref.12].

5. Bahamas: [reef; mH; Fall, mPG]
An extensive erosional surface has been described from two islands in the Bahamas (San Salvador and Great Inagua islands)[15–20] and an intra-LIG unconformity has been mapped for 5 km in West Caicos[21] (in the nearby British West Indies, see section 5.1 below). In the

Bahamas, this erosional surface, with shallow-water borings and burrows, separates two LIG reef units. On San Salvador, the Cockburn Town reef erosional surface truncates coral-rubble calcarenite and *in situ* corals. This surface is also encrusted with shallow water borings and burrows and occasionally a palaeosol (red caliche) is preserved[16,17]. On Great Inagua, the Devils Point reef erosion surface extends over several kilometres and again truncates coral-rubble calcarenite and *in situ* corals. The surface has lithophagid and sponge borings with rhizomorphs encrusting the surface. This erosional surface in turn is overlain by LIG corals[15–17]. The initial reef unit formed at ~+4 m above present mean sea level (apmsl) and the intra-LIG event is dated at ~125 to 124 ka and lasted <1.5 ka[Ref.15], followed by a sea-level fall of ~4 m and subsequent sea-level rise of ~+6 m[Refs.15–17]. However, preservation of delicate reef-crest facies[22,23], the apparent lack of *Acropora palmata* reef crests above +3 m, and inter-tidal notches preserved at +6 m[Ref.22] led Hearty and Neumann (2001)[Ref.24] and Neumann and Hearty (1996)[Ref.22] to suggest that the ~+6 m sea-level highstand was of short duration and occurred at the end of the LIG, rather than during an extended episode of elevated sea levels. These authors suggested that the late stage, m-scale sea-level rise was too brief to permit reef development[22]. Blanchon et al. (2009)[Ref.25] noted the similarity in magnitude of the sea-level 'jump' (~3 m) between the Bahamas and Yucatan Peninsula, and suggested that the lack of reef crests at elevations >3 m is due to processes other than sea-level rise. Recent open-system U-series age determinations on *in situ* corals[19] from the superimposed reef units from San Salvador and Great Inagua islands suggest at least one sea-level oscillation during the LIG highstand - "Bahamian geochronology and stratigraphy indicate four resolvable units, supporting the four oscillations in sea level recorded in Red Sea core KL11 (Rohling et al., 2008). There is a 4 ± 1 kyr age difference between Reefs II and I, which are separated by a wave-cut bench, providing definitive evidence of a sea-level oscillation (White et al., 1998; Wilson et al., 1998; Chen et al 1991)"[Ref.19]. However, recent work could not identify these four units, but "found compelling evidence for at least two distinct generations of reef growth, separated by an ephemeral sea-level fall" (Skrivanek et al., 2018)[Ref.20]. Conventional (i.e., closed-system) datings have so far been unable to differentiate between the ages of the two reef units separated by the erosional surface[15], although the youngest closed-system ages for the lower reef unit (Reef I) are ~124.5 to 125 ka[Ref.20].

5.1 West Caicos, British West Indies [reef; mH; Fall, mPG]
An exceptionally preserved exposure of LIG reef sequence (with distinct lower and upper reef units, with ages of ~126.5 and 120.6 ka respectively) has been mapped over ~8.4 km along the west coast of West Caicos island[21]. The lower/early-LIG unit is a fringing reef, with *Acropora palmata* core and coralline algal crust indicating sea levels of ~+4 m at 126.5 ka. An intra-LIG unconformity (mapped over 5 km) with clear evidence for erosion of the lower reef platform, suggests a brief sea-level fall. In places the lower reef unit is truncated by ~3 to 4 m, suggesting that the intra-LIG sea levels fell to ~+1 m or lower. The upper (superimposed) reef unit is capped with foreshore deposits at ~+5 m elevation (unabraded corals that colonised the erosion surface were dated to 120.6 ka). Following this second highstand, progressively downstepping shorelines document falling sea levels.

6. Bermuda: [reef; ?]
The Devonshire Marine Member (aka Rocky Bay Formation) has been correlated with MIS 5e[e.g., 26,27] and is separated from the underlying Belmont Formation by a solution unconformity/soil pipes/reddish soil-like deposits. The age (and hence sea-level interpretation) of the Belmont Formation is contested[e.g., 28,29]. At Grape Bay, the contact

between the Belmont Formation (U-series dated to the penultimate interglacial) and the Devonshire Marine Member is marked by a geosol/soil pipes suggestive of a period of subaerial exposure prior to deposition of the LIG Devonshire Marine Member[29]. Hearty and Kindler (1995)[Ref.23], and Hearty (2002)[Ref.30] (reiterated by Hearty et al., 2007[Ref18], and Hearty and Tormey, 2017[Ref.28]) reassigned the Belmont Formation to a member of the Rocky Bay Formation (correlated with MIS 5e[Ref.26]). As a consequence, these authors propose an intra-LIG sea-level fluctuation (i.e., two highstands[23]). However, recent consensus (based on U-series dating of coral fragments) suggests that the Belmont Formation formed during the penultimate interglacial[26,27,29], rather than during the LIG[18,28,30].

7. Florida: [reef; Fall?, mPG]
Within the Key Largo Formation (emerged coral reef-facies limestone with a maximum elevation ~5.5 m above mean high tide) five distinct units are recognised, and are separated by surfaces that indicate subaerial exposure (Q5 correlates to the LIG[e.g., 31]). At Windley Key, Fruijtier et al. (2000)[Ref.32] documented an erosion surface. A coral (sampled at ~+3 m above mean high tide) below this erosion surface was dated to 125 ka. However, this sample has a calculated $\delta^{234}U_{initial}$ value outside of the modern range despite low percentage calcite and ^{232}Th concentration. Diagenetic alteration during the first 40 ka after formation is thought to account for generally older than expected ages at the site[32]. The Miami Limestone (ooid shoals or bars and correlative of the LIG Key Largo Formation) reaches a maximum elevation ~+7.5 m apmsl. An unconformity at ~1.2 m apmls separates two oolitic units[Refs.31,33]. However, an intra-LIG sea-level fluctuation was not recognised from a subsequent stratigraphic and dating study[31].

8. Hawaii: [reef; mH,? Fall?, mPG]
A continuous sequence of strata exposed at Barbers Point, Oahu, includes two stratigraphically distinct highstand units (units II and V) that are separated by "a regressional sequence including *in situ* slabs of beachrock"[Ref.34]. Initial U-series ages of the two marine units suggest a gap of several thousand years between deposition of these two layers[34]. Elsewhere on Oahu, the top of the Waimanalo Formation (U-series dated to the LIG [e.g., 35,36]), an *in situ* coral-algal framestone, is often planar (e.g., Costa Dairy, now quarried away[18,37]) and in some instances erosionally truncated on its upper surface. This "erosional unconformity" represents the mid MIS 5e lowstand and separates the framestone from overlying grainstone and rudstone (Leahi Formation) that accumulated during the second 5e highstand)[34]. Mokapu Point (east coast of Oahu) contains two stacked *in situ* coral reefs, separated by a terrigenous basalt conglomerate, with no evidence of subaerial exposure. Similarly, the Kahe Beach State Park sequence includes two exposed *in situ* "reef levels" capped by marine conglomerate[18].

Amino acid racemization (AAR) dating of the Waimanalo Formation[38] appears to confirm the age separation of the two marine units[cf. 34] and was used as further evidence for two sea-level highstands separated by a minor regression. Subsequent U-series dating of the various LIG units confirm a LIG age, but unit ages are largely indistinguishable from one another[18,29,35,36,39] and "fail to corroborate the exquisite lithostratigraphic succession of this site, as most ages do not pass reliability standards"[Ref.18], yet Muhs et al. (2002)[Ref.29] "do not see any persuasive evidence for two separate high stands… as interpreted by Sherman et al. (1993) from elsewhere on Oahu".

9. Western Australia: [reef; Fall, mPG]
(see also section 12 for discussion of LIG coral evidence)
A sharp unconformity (erosional surface/abrasion platform formed within a LIG rocky shore) has been documented within the Tamala Limestone Formation (Cape Burney, near Geraldton)[40]. This low-relief, channelled surface formed on calcareous sandstone and is encrusted by intertidal to shallow subtidal biota (coralline algae, serpulid worms) and coral. It is overlain by a reef unit dominated mostly by undisturbed coral fronds of robust *Acropora* species[40]. However, the age and sequence of events, particularly the late LIG highstand in Western Australia, remain controversial.

10. Mediterranean
Multiple sites within the Mediterranean are inferred to contain evidence of LIG sea-level oscillations. A thorough review of this literature is beyond our scope, and only a brief discussion of key sites is given. The Mediterranean has a complex tectonic setting but small tidal amplitude and low wave energy. Evidence of former sea levels comes from a range of sea-level archives - depositional (beach or shallow marine deposits[e.g.,41–43], geomorphological (shore platforms or notches) or fixed biological indicators[e.g., 44]. Dating of deposits is challenging because there are few corals for U-series dating and this technique is unreliable when applied to fossil molluscs[e.g., 45]. We do not reinterpret or recalculate ages from the original publications and instead concentrate on the stratigraphic evidence for potential sea-level oscillations. Due to the problems of obtaining reliable age control for Mediterranean Quaternary sediments, fossil mollusc assemblages (e.g., the warm "Senegalese fauna"[e.g., 46]) are often used to identify LIG deposits (due to their temperature sensitivity), with *Strombus bubonius* (*Persististrombus latus*), which is extant in the tropical waters off west Africa but not in the Mediterranean today, particularly diagnostic[e.g.,45]. It should be noted that some authors[e.g., 43,46] suggest that this fauna is neither synchronous nor continuous throughout the Mediterranean during MIS 5e[Ref.46] and it has also been found in older interglacial deposits[e.g., 43], although these conclusions are based on U-series dating of fossil molluscs[45].

The complex Mediterranean tectonics, coupled with dating uncertainty, has made deconvolution of LIG sea-level history of the basin difficult. For example, only one highstand is recognised in the "generally stable" tectonic setting of Sardinia based on tidal notches with a mean elevation of +6 ± 3 m (apmsl) (Ferranti et al. (2006)[Ref.47] and references therein), and from shoreline evidence from multiple Mediterranean sites[42,48], whereas multiple highstands are inferred for sedimentary sequences elsewhere in the basin[e.g.,43,46,49,50].

10.1 Italy (including Sardinia & Sicily): [notches; mH?, oscillations?]
Emerged tidal notches, including "double notches" (tidal notch couplets) or superimposed bioerosional grooves, are preserved at many sites in Italy due to the microtidal regime[44,47,51]. The upper notch is commonly attributed to MIS 5e and the lower to later stages within MIS 5, although firm age control remains elusive. Superimposed bioerosional grooves associated with upper notches at ~+5 m elevation in the Gulf of Orosei and Bergeggi Marine Cave (+5.24 m, +4.40 m, +3.52 m and +2.7 m elevation) are thought to have formed during distinct highstands within MIS 5e [Ref.44]. However, Antonioli et al. (2006)[Ref.51] argue that both notches of the tidal notch couplets formed during the LIG, with the lower notch forming during the earlier portion of the LIG, although this was attributed to glacio-isostatic adjustment (GIA) processes, rather than sea-level fluctuations and hence the different morphology of the two notches within the couplet[51]

10.2 Israel (Galilee coast): [sedimentary sequence; mH; stillstand/Fall]
The Rosh Hanika site is a micro-tidal, tectonically stable location that contains a complete stratigraphic sequence for MIS 5e, although U-series ages from molluscs are altered (open-system)[50]. The continuous shore sequence is as follows (generalised from sites in the wider region, with only the Rosh Hanika site containing the complete stratigraphic section): first comes the the Regba Member, a calcareous sandstone (aeolian dune, tentatively ascribed to MIS 6, with upper planar beds characteristic of a shallow marine or coastal environment). In some locations (e.g., Hazrot Yasaf) abrasion platforms are evident (at +2.6 m and +3.4 m apsl), which were cut by tidal channels. The authors suggest that these were cut during relatively long sea-level stillstands as part of two sea-level-rise steps within an initial MIS 5e sea-level rise (see note below *). The Regba Member is overlain unconformably (interpreted as a sea-level drop) by the Yasaf Member, which contains a gravel unit with *Strombus bubonius* fossils (warm water fauna used as a marker of MIS 5e in the Mediterranean). This is in turn truncated by an unconformity, which is inferred to have been caused by a sea-level fall that caused a relatively short period of emergence, and which is in turn overlain by a *Vermetidae* reef (indicative of a low energy environment) capped by algal crust (inferred shallow water deposition). There is another unconformity (cessation of reef formation, likely due to sea-level lowering), that is overlain by two bioclastic sandstone subunits (subsequent transgression). After this, sea level dropped and the coastline retreated offshore[50].

* Abrasive notches exposed along the Galilee coast suggest sea levels slightly higher than present at the start of MIS 5e, with an upper limit between +0.5 to +0.75 m. The notches contain two subunits of the Yasaf Member, which indicate relatively long stillstands at an elevation of ~+1 m, and that the early MIS 5e erosive phase was followed by a depositional phase later in MIS 5e[Ref.49].

10.3 Tunisia: [sedimentary sequence; mH?, Fall?]
The Hergla site in Tunisia contains a facies succession that includes two foreshore deposits, each overlying a possible erosion surface[18,52,53]. The lower unit is a siliciclastic unit devoid of warm water fauna (~+2 to +3 m apmsl, aged 147 to 110 ka from U-series dating of molluscs) capped by aeolian sediments that are overlain by a carbonate-rich, shallowing-upward marine unit that contains warm marine fauna including *Strombus bubonius* (ages derived from U-series dating of *Ostrea lamellosa* shells range from 141 to 100 ka), capped by a *Strombus*-rich boulder bed (elevation ~+3 to +6 m apmsl)[52]. These units are interpreted as two MIS 5e highstand deposits that developed during two sedimentation phases, during two distinct sea-level highstands based on sedimentology, faunal assemblages and U-series dating of molluscs/a coral, and amino-acid dating[18,41,52,54]. Hearty et al. (2007)[Ref.18] interpreted the top of the aeolian deposit (capping the first unit) to be a weathering surface associated with a sea-level fall "to near or below present", whereas Mauz et al. (2018)[Ref.53] relate this to lagoonal sediments, which suggests shoreline migration. Recent OSL dating of the lower (110 and 120 ka) and upper units places the sea-level rise associated with formation of the second package in MIS 5a, rather than a second LIG highstand[Ref. 53].

10.4 Spain: [sedimentary sequence; mH; Fall]
A variable number of highstands associated with MIS 5e is recognised on the Spanish coast[e.g., 55], with the greatest number documented on the Mediterranean coast (primarily due to tectonic uplift)[e.g., 56]. Three LIG highstands for the Iberian Peninsula have been inferred based on extensive geomorphological mapping, dating and facies analysis[e.g.,43,46,57]. The general sequence is: (1) a first LIG highstand (characterised by oolitic dunes and beaches containing

Strombus bubonius), (2) a second highstand with the highest elevations and containing "two morphosedimentary subunits separated by an erosional surface"; and (3) a brief third highstand in which sea level was slightly lower[55]. For example, the Loma del Viento section[43,58,59] contains a laterally extensive 'staircase' of marine units, four of which contain *Strombus bubonius.* These are terraces 12, 13, and 14 with present elevations +14, +6, and +3 m apmsl, respectively (following the stratigraphic subdivisions of Zazo et al. (2003)[Ref. 43]) and three LIG sea-level oscillations are proposed based on U-series and AAR dating[58–60]. Similarly, the El Pinet site (an abandoned quarry) contains five prograding units (numbered 7.1 to 7.5 in Zazo et al. (2003)[Ref.43]), all containing the warm "Senegalese" fauna and *Strombus bubonius*. Unit 7.1 (sepulid/bioclastic limestone with patches of encrusting coral indicative of shallow marine environments, assigned to MIS 7) is overlain by an oolitic calcarenite. An erosional layer separates unit 7.2 and overlying siliclastic sandstones and conglomerates (unit 7.3). Erosional layers also separate LIG unit 7.3 and overlying units 7.4 (calcarenite) and 7.5 (calcarenite, sandstones and conglomerates which is the "richest" in *S. bubonius*)[43].

10.5 Balearic Islands – Mallorca: [sedimentary sequence; mH?, Fall?]
Emergent marine deposits (elevations of +2 and +3 m apmsl) that are dated (or inferred) to be of MIS 5e origin are documented from several locations on Mallorca[41,43,46,48,57]. Two (and possibly three) distinct sea-level highstands are proposed during the LIG, one early at ~135 ka and two at ~117 ka[Refs.41,43,46,57], although these ages (except Hearty, 1986[Ref.41]) are based on potentially unreliable U-series mollusc dating. The ages and elevations of the marine deposits correspond to speleothem (phreatic) overgrowths from coastal caves at elevations of +1.5 m to +2.6 m dating from ~138 to 110 ka[Refs.61–63]. Tuccimei et al. (2007)[Ref.64] proposed that two episodes of speleothem growth are separated by a rapid LIG regression/lowstand at ~125 ka. At the Campo de Tiro site, marine units (~0 to +3 m elevation apmsl) are separated by reddish terrestrial deposits or erosional surfaces[41,43,57]. However, the precise age and number of LIG sea-level oscillations (highstands) at this site are debated. Hearty (1986)[Ref.41] recognised three marine units, whereas four marine units were documented by Bardají et al. (2009)[Ref.46], Hillaire-Marcel et al. (1996)[Ref.57] and Zazo et al. (2003)[Ref.43].

A marine unit (unit 2 of Zazo et al. (2003)[Ref.43]); max elevation ~+3 m[Refs. 43,48]) is underlain by a thick red silt layer. Note that Zazo et al. (2003)[Ref.43] also assign the marine unit below this silt layer (elevation +1.5 m apmsl) (unit 1) to the LIG due to the occurrence of warm-water fauna, including *Strombus bubonius*, in both units, whereas Muhs et al. (2015)[Ref.48] attributed the aeolianite, from which the palaeosol developed, as likely formed during MIS 6. The third marine unit of Zazo et al. (2003)[Ref.43] and Bardají et al. (2009)[Ref.46] (unit 3, elevation of +1 m apmsl), also contains warm-water fauna but without *S. bubonius*, overlies an erosional surface that truncates both units 1 and 2. However, this unit was not recognised in the later fieldwork of Muhs et al. (2015)[Ref.48]. In contrast, Muhs et al. (2015)[Ref.48] documented seaward "Neotyrrhenian" beds (max. elevation +2 m apmsl) that consist of a lower layer of gravelly sands (with few fossils) and an upper sandy gravel layer containing abundant fossils. These beds overlie a reddish-brown palaeosol, which was found to be a aeolianite, which is in turn overlain by marine deposits documented at +3 m. These seaward "Neotyrrhenian" beds were interpreted as a beachrock facies that formed later during the same highstand as the +3 m marine deposits[48].

U-series dating of molluscs and stratigraphic evidence led Hillaire-Marcel et al. (1996)[Ref.57] and Zazo et al., (2003)[Ref.43] to suggest a MIS 5e origin for all three marine units (units 1, 2, and 3), in which the youngest was assigned to a separate, later LIG highstand based on facies

and faunal considerations[43]. U-series dating of fossil corals and amino-acid dating of molluscs from the uppermost portion of the "Neotyrrhenian" beds suggest an age of ~120 to ~123 ka for this deposit[41,48], but Muhs et al. (2015)[Ref.48] consigned all the marine units to the same highstand despite the different sedimentology of the two marine deposits. Glacio-isostatic processes were invoked to account for the two marine units by Muhs et al. (2015)[Ref.48], given the small altitudinal separation (~1 m) between the documented marine units.

10.6 Canary Islands: [sedimentary sequence; mH, Fall]
Marine deposits containing *Strombus bubonius* have been documented at low (<12 m) elevations on many Canary Islands[43,65], but robust age control is lacking. On Lanzarote (El Berrugo), three stratigraphically superimposed MIS 5e units with a sharp erosional surface between units 2 (calcarenite containing *Strombus bubonius*) and 3 (cemented conglomerate including pebbles eroded from earlier units, interpreted as a beach deposit) were used to suggest subaerial exposure prior to deposition of unit 3 during the LIG, possibly indicating two highstands[43]. On Fuerteventura Island, the stratigraphic section at Rosa J. Sánchez site contains alternating marine (3 units) and terrestrial (two) units, with U-series dating of mollusc shells suggesting MIS 5e ages for all marine units[43]. The Playa de Igueste site (Tenerife) comprises two superimposed marine units; the lowermost marine (conglomerate) unit contains *Strombus bubonius* and is separated from the upper marine unit (beach conglomerate also containing *Strombus bubonius*) by a terrestrial silty deposit, which suggests the presence of two MIS 5e highstands interrupted by a possible period of sea-level lowering[43].

(1B) REEF ARCHITECTURE
11. Yucatan, Mexico: [reef; oscillation - sea-level "jump", mPG]
A laterally extensive back-stepping LIG reef sequence has been documented[25,66] from a tectonically stable site. The complete reef sequence consists of "two separate linear reef tracts with reef crests that are offset and at different elevations"[Ref.25]. This backstepping sequence was used by Blanchon et al. (2009)[Ref.25] to suggest sea-level instability (a sea-level "jump") during the later stages of MIS 5e at rates similar to those in the Caribbean during the last deglaciation (~ 36 mm/yr)[Refs.67,68]. Currently, the reefs lack good age control, but biofacies and stratigraphic evidence suggest that both reef units are contemporaneous and that the lower unit if older, died suddenly but remained submerged while the upper reef unit back-stepped during sea-level rise, i.e., "reef development during the highstand was punctuated by reef-crest demise at +3 m and back-stepping to +6 m. The abrupt demise of the lower reef crest, but continuous accretion between the lower-lagoonal unit and the upper-reef crest, allows us to infer that this backstepping occurred on an ecological timescale and was triggered by a 2-3 m jump in sea level" [Ref.25].

12. Western Australia: [reef, mH, stillstand, mPG]
A well-developed MIS 5e terrace is documented at ~+2 to +4 m elevation (apmsl) along extensive portions of the Western Australian coastline [69–75]. At Cape Cuvier, two "geomorphologically distinct" MIS 5e marine highstand units—a lower erosional fringing reef (shore platform, formed by wave abrasion in middle to upper intertidal zone elevations at ~+2 m to ~+3.6 m apmsl) and an upper, narrow "underdeveloped" constructional reef at +8 to +10 m apmsl—were used to argue for an extended sea-level stillstand followed by a short-lived excursion of elevated sea level at the end of LIG, reaching perhaps +8.2 m (or even +9.4 m) apmsl late in MIS 5e[Refs.72,74]. In the Shark Bay area, a possible sea-level

regression was suggested given an apparent 'age gap' and inferred abrupt halt in coral growth at ~124 ka[Ref.73]. However, the ages and sequence of events, particularly for the late LIG highstand in Western Australia, remain controversial. Many U-series ages for the LIG in the Australian region suggest pervasive open system behaviour and/or variable diagenesis[e.g., 70,71]. In addition, the +5 to +6 m emergent shoreline mapped at Quobba Ridge (inferred palaeo sea level of +9 m after GIA correction[74]) and the Cape Cuvier upper terrace/rim[72,74] are thought to result from significant neotectonic deformation rather than sea-level fluctuations[76].

13. Haiti: [reef; mPG]
Dumas et al. (2006)[Ref.77] mapped two LIG terraces (T3a and T3b), separated by ~2 m in elevation from a tectonically uplifted terrace sequence[77,78]. U-series dating for the lower terrace gave an age of ~130 ka (inferred relative sea level +5 m apmsl), with the upper terrace dated to ~118 ka (sea level + 2.7 m apmsl). These two sub-terraces are not always distinguishable, and the localised expression is thought to relate to the higher uplift rate at the site surveyed by Dumas et al. (2006) compared to other surveyed sections in the area[78], where the two terraces merge into each other[77].

14. Barbados: [reef; mH; mPG]
The Rendezvous Hill terrace is an emerged LIG reef complex that retains much of its original depositional morphology. Stratigraphic evidence for LIG sea-level instability from the fossil reef is equivocal but some authors have proposed multiple sea-level peaks based on morphology, facies information and dating[18,79,80].

Based on reef morphology and ESR dating, three episodes of constructional reef-terrace formation during the LIG have been proposed[81]. Terrace dating suggests that terrace T5a (~128 ka) and terrace T5b (~ 132 ka) formed during an initial LIG highstand, whereas terrace T4 formed at ~ 118 ka when sea level was several metres below present (ages as originally reported). However, a younger age for the two higher terraces (terraces T5a and T5b) and an older age for the lower T4 terrace (also known as the Maxwell terrace) were obtained using whole-rock amino acid dating[18], which led these authors to correlate the lower T4 terrace with an initial LIG highstand, and the T5 units to a subsequent, higher sea-level highstand during the LIG.

A multi-stage LIG reef development was also suggested from reef-front-architecture variations and facies relationships[79]. Using a detailed facies approach, these authors suggest that a brief episode of rapid sea-level fall and possibly a minor stillstand led to the reef development at ~16 m below the original reef crest (cf. Maxwell terrace/T4 terrace of Schellmann and Radtke, 2004). However, lack of duplicate reef architecture suggested that any LIG oscillations must have been rapid (hence the lack of a constructional reef record)[Ref.79]. A sea cave at +6 m is thought to have been cut during the LIG, and was used to infer reef-growth cessation prior to the peak (maximum) sea level, possibly due to a change in environmental conditions or a jump in the rate of sea-level rise (rate of rise > rate of reef accretion)[Ref.79].

(1C) CHALLENGES OF REEF STRATIGRAPHY
Reef accretion is complex and results from an interplay of many factors that includes physio-chemical parameters (irradiance, temperature, hydrodynamic energy etc.), the composition of reef communities and their potential rates of growth/bioerosion, balance between

sedimentation vs. calcification, reef disturbance (storms etc.), and variations in coral recruitment, as well as the rate and amplitude of sea-level change (for further discussion, see the reviews of Scoffin *et al*., 1980[ref.82], Montaggioni, 2005[ref.83], Hubbard, 2009[ref.84], Woodroffe and Webster, 2014[ref.85], Camoin and Webster, 2015[ref.86], Hibbert *et al.,* 2016[ref.87]). In addition, taphonomic and diagenetic processes, and potential coring artefacts, have implications for interpreting spatial variation and the rates and style of framework development[88–92]. For example, coral skeletons are frequently reworked in many reef settings, with selective destruction of certain growth forms, individuals, and age-classes, as well as a mixing of successive generations (also known as time averaging – both ecological and sedimentological[e.g., 88,93,94]). Reworking by storms/hurricanes etc. can also exert a strong control on reef anatomy, such that *in situ* framework is lacking, and instead the reef consists of coral-cobble rudstone layers (e.g., Blanchon et al., 1997[ref.95]). The latter led Hubbard et al. (1990[ref.96]) to state that, for many reefs in the Caribbean, "…the importance of detrital material in the reef fabric and the major role played by secondary processes that constantly rework the substrate have resulted in a reef whose interior is more of a "garbage pile" than an in-place assemblage of corals cemented together into a rigid framework."

Given the interplay of some or all of the above-listed processes, complex age structure is possible and is an important limit on the temporal precision achievable from reef-based sea-level reconstructions[97]. Individual dates from a reef unit that represents a certain time-interval may be stratigraphically jumbled within the unit. Such complex age structures have been reported, for example, for Holocene growth on the Great Barrier Reef[98,99]) and Papua New Guinea (Huon Penninsula[97]).

(1D) SYNTHESIS

The nature of LIG sea-level variability remains strongly debated[e.g.,18,100]. Different models of LIG sea level have been proposed from coral records. These include:

a) relatively stable sea level (i.e., one major peak) (e.g., Stirling et al., 1998[ref.71]);
b) two peaks separated by a sea level fall of various magnitudes (e.g., Chen et al., 1991[ref.15], Stein et al., 1993[13], Sherman et al., 1993[ref.34], Plaziat et al., 1998[ref.4], Bruggemann et al., 2004[2], Thompson and Goldstein 2005[ref.80], Hearty et al 2007[ref.18], Kerans et al., 2019[ref.21]);
c) relatively stable (possibly with a small drop) sea level with a rapid late rise (e.g., Neumann and Hearty, 1996[ref.22], Hearty, 2002[ref.30], O'Leary et al., 2013[74], Blanchon et al., 2009[ref.25]) and;
d) multiple peaks (e.g., Thompson et al., 2011[ref.19], Rohling et al., 2008[ref.101], this work).

The intensively studied, sampled, and dated LIG coral/reef records of the Seychelles[8–10], Bahamas[15,19], and Western Australia[18,70–74] give an emerging picture of LIG sea level that have similarities with the Red Sea record. These coral records are especially useful given that: (1) they span extended periods of the LIG, (2) they have relatively high temporal sampling and density of radiometric dating, (3) they are from tectonically stable areas; (4) they have well-documented stratigraphic superposition of LIG units, and (5) for the Seychelles, there are well-constrained palaeo-water depth estimates. We do not view these records in isolation, but within the well-documented context of the records extensively discussed in sections 1A and 1B.

The GIA corrected Seychelles corals document an initial gradual eustatic sea level rise from ~+5.9 ± 1.7 m to +7.6 ± 1.7 m between 129 and 125 ka, with a possible drop before 125 ka.

A single encrusting coral at +9.2 m at ~125 ka from Camp Rock, Cape Cuvier in Western Australia suggests "a rapid 3 m rise … and fall in sea level at this time"[Ref.74]. Both the Bahamas and Seychelles suggest sea level at ~4 m at ~123 and possibly 124 ka[Refs.9,19] with a decrease (drop) in sea level to ~0 m between 123 and 119 ka in the Bahamas[19]. Sea level highstands at 119.2 ± 0.5 ka (about 6 m), 117.5 ± 0.4 ka, and 114.4 ± 1.0 ka are seen in the Bahamas record as four distinct stratigraphic units, and the possibility of a sea-level drop between each highstand cannot be discounted[19]. A final (and somewhat contentious, given the tectonic setting and potential open-system behaviour) sea-level high of +3.4 m (GIA corrected) at ~118.1 ± 1.4 ka in Western Australia[74] may correlate with either the 119 ka or the 117 ka Bahama deposits[19]. The Barbados coral record[102] is often used to constrain the 'age' of the MIS 5e/d transition. In this study, the ages and elevations of two corals OC4 and OC-1 (dated in triplicate and each satisfying age reliability criteria) bracket the sea-level fall at the end of the LIG. The youngest coral gives a youngest age constraint for the LIG-end at ~113 ka. Yet, in tectonically stable locations, no LIG corals are found that are younger than: (1) ~114 ka in Florida[31]; (2) ~118 ka in the Bahamas[19]; and (3) ~ 117 ka in Yucatan Peninsula[25]. Similarly, speleothem growth began (as a result of sea level fall) at ~ 116 ka in Mallorca[61,62] and was below -4.9 m at 117 ka in Yucatan Peninsula[103].

Supplementary Note 2.

LIG age adjustment in the Red Sea sea-level record

Here we show details of the LIG age adjustment, which is primarily driven by comparison of the overall Red Sea stack record with the Yucatan speleothem-based indications of when sea level first dipped below 0 m again[103], and secondarily by indications from coral-data compilations of when the LIG ended[102,104]. The Red Sea stack is shown on its previous age model in *Supplementary Figure 2* (left). This age model was found to be deficient for the end of the LIG, and comparison with the aforementioned benchmark records reveals that the LIG end is better placed at ~118.5 ka, noting the generous 2σ (95%) uncertainty of ±1.2 ka that applies to the Red Sea age model (*Supplementary Figure 2* bottom; *Supplementary Figure 3*). To make this adjustment, and evaluate its uncertainties, GIA impacts were considered (*Supplementary Figure 4*).

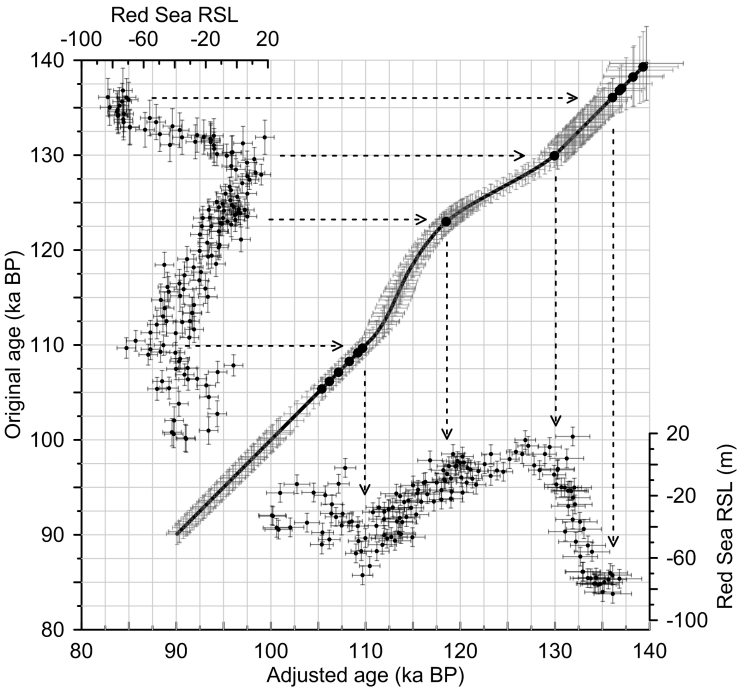

Supplementary Figure 2. Interpolation and propagation of age uncertainties for the adjusted Red Sea Last Interglacial chronology. Elements shown include: the Red Sea sea-level stack on its first radiometrically-controlled chronology[105,106] (left); the adjusted age-control point (central dot at 123 ka on the Y axis, which becomes 118.5 ka on the X-axis, as per adjustment of the 95% upper limit to the coral- and speleothem-based end of the LIG highstand at 118.5 ka; see Figure 2); a number of forced age-control points to effect exact agreement between the chronologies >130 ka and <110 ka (other dots on the 45° line – this ensures that, outside the LIG adjustment interval, the new chronology is identical to the original chronology); and the Red Sea sea-level stack on its adjusted chronology (bottom). Interpolation and uncertainty propagation for the adjusted chronology is described in *Methods.* Arrows visualise the adjustment pathway.

For this analysis, we corrected both the Red Sea record and the Yucatan Peninsula speleothem record for GIA processes using configurations of the penultimate glacial (MIS 6) ice sheets after Rohling *et al.* (2017)[ref.107]. These use a smaller Laurentide Ice Sheet with either: (i) a Eurasian Ice Sheet (EIS) with greater mass but LGM-like spatial configuration; or (ii) an EIS with both greater mass and spatial extent. Fuller details of the chosen Earth model and ice models are given below in *SI Part 4*, where it is shown that the GIA corrections themselves have uncertainties up to ±3 m at the end of the LIG. The exercise used here for evaluating the Red Sea versus Yucatan record after GIA correction uses an artificially defined Global Mean Sea Level (ice-volume) history. Results show that the Yucatan record closely tracks GMSL (*Supplementary Figure 4*). The Yucatan data indicate that Yucatan RSL (and thus by close approximation GMSL) first reach −4.9 m just after ~118 ka (*Supplementary Figure 3*). The upper 95 % confidence bound for Red Sea RSL would sit some 3 m above that (*Supplementary Figure 4*), with an uncertainty up to ± 3 m (*Supplementary Figure 5*); hence our selection of the ~118.5 ka age for the upper 95% bound of the Red Sea record to fall through 0 m. Bearing in mind the generous 2σ (95%) uncertainty of ±1.2 ka that applies to

the Red Sea age model (*Supplementary Figure 2*), this selection of ~118.5 ka is coherent with both the Yucatan data[103] and the Cutler et al. (2003)[102] and Hibbert et al. (2016)[83] coral-based assessments for the LIG end.

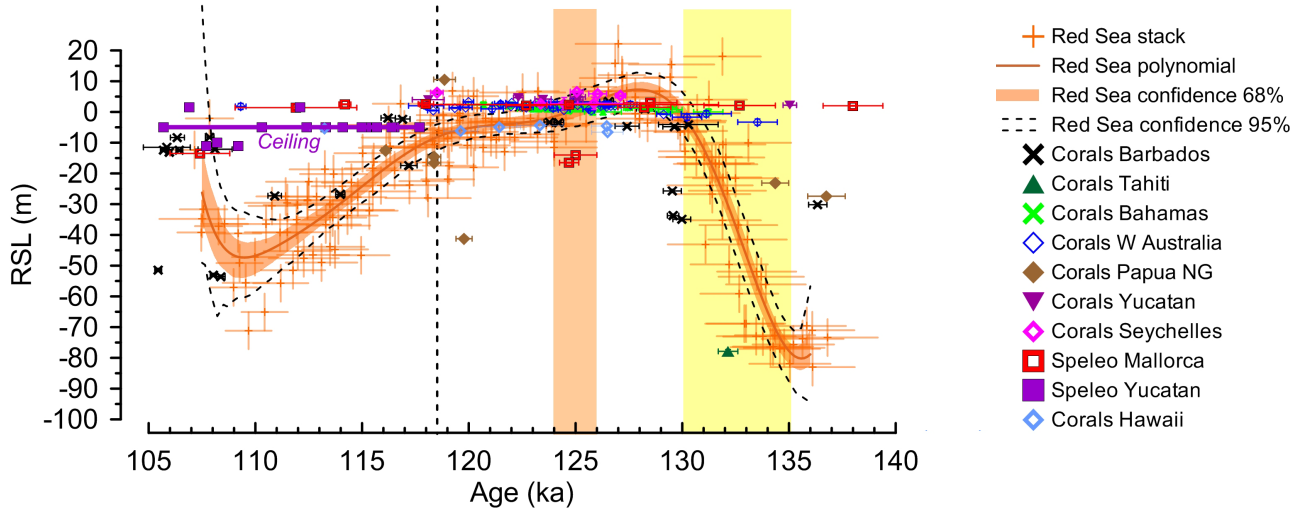

Supplementary Figure 3. Red Sea, coral and speleothem sea-level data. Red Sea stack of relative sea-level (RSL) data with 1σ error bars, polynomial smoothing and 68% and 95% confidence intervals. Coral data, from the compilation of Hibbert *et al.* (2016)[Ref. 87] and Dutton *et al.* (2015)[9], are reported in ka BP, where all coral ages were recalculated (when necessary) using the Cheng *et al.* (2013)[Ref.108] decay constants for ^{234}U and ^{230}Th and assuming closed system behaviour. Corals have been screened for age 'reliability' using the following criteria: calcite <2%, ^{232}Th concentrations <2 ppb, and a calculated $\delta^{234}U_{initial}$ in the range of modern corals (i.e., $\delta^{234}U_{initial}$ = 147 ± 5 ‰). Replicate ages passing the screening criteria are have been averaged (using an inverse weighted mean). Corals are from: the Bahamas[15,19] (green cross); Barbados[79,109–112] (black cross); Tahiti[113] (dark green filled upward pointing triangle); Yucatan Peninsula[25] (purple filled downward pointing triangle); Seychelles[8,9] (pink open diamond); Hawaii[29] (blue open diamond); and Western Australia[69–71,73,75,114] (dark blue open diamond). The Seychelles point at 118 ka is an inverse weighted mean of samples SY-22c (112.2 ± 0.61, 2σ, including decay constant error) and SY22a (124.3 ± 0.56 ka, 2σ, including decay constant error) from site 4 in Dutton *et al.* (2015)[ref.9] (their Table 3, SY-22a 124.5 ± 0.5ka; SY-22b 96.1 ± 0.4 ka; SY-22c 112.4 ± 0.6 ka). Although Dutton *et al.* (2015)[ref.9] remove SY-22a from subsequent analysis as they suspect U-addition, both the SY-22a and SY-22c replicate samples pass our screening criteria, so that we have no objective criterion to eliminate one or the other. We simply plot the mean, but flag a potential issue. Speleothem evidence of past sea levels from phreatic overgrowths from Mallorca[61,62,115] (red open squares) and subaerially deposited speleothems from the Yucatan Peninsula, Mexico[103] (purple filled squares, subaerial growth indicated by solid purple line marked 'ceiling'). Yellow bar denotes the time-interval of Heinrich Stadial 11 (HS11)[116]; orange bar indicates the time-window of potential short-lived sea level lowering observed in, e.g., the Seychelles[8,9] and Red Sea[3,this study]. The relationship between the initial (orange) polynomial assessment of the entire Red Sea stack and the more precise probabilistic assessment of core KL11 alone is illustrated in Figure 2.

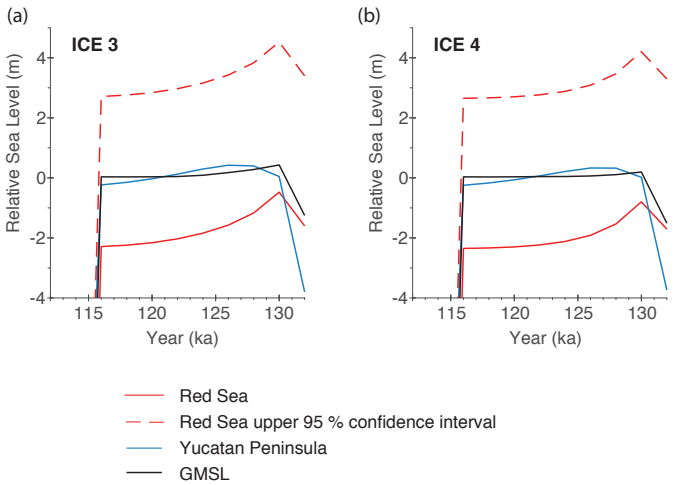

Supplementary Figure 4. Glacio-isostatic adjustment modelling of Yucatan Peninsula speleothem and Red Sea record. GIA predictions of relative sea level for the Red Sea stack (solid red line = median; dashed red line = upper 95 % confidence interval), Yucatan Peninsula (blue) and global mean sea level (GMSL, black) using 'more realistic' MIS 6 ice histories. We use a VM-2-like earth model, a smaller volume Laurentide Ice Sheet and: (a) greater volume Eurasian Ice Sheet with LGM-like spatial configuration (ICE 3); and (b) greater volume Eurasian Ice Sheet with more extensive spatial extent (ICE 4).

Supplementary Note 3.

Greenland mass loss estimates from East Greenland Current sea-water $\delta^{18}O$

Sediment core MD03-2664 (57°26.34'N, 48°36.35'W; 3,440 m water depth) from Eirik Drift[117,118], off the southern tip of Greenland, lies under a system of surface currents that carry most of the melt contribution from the Greenland ice sheet, most notably the East Greenland Current and the wider Labrador Sea systems. Today, Greenland meltwater affects the net seawater $\delta^{18}O$ by addition of water with salinity (S) of 0, and $\delta^{18}O$ of around −30‰. Other (almost) freshwater components, with typical property values are sea-ice melt (typically S = 3, $\delta^{18}O$ equal to ambient water plus 2.1‰), and meteoric water from precipitation and river input (S = 0, $\delta^{18}O$ = −18‰). These mix with ocean water advected to high latitudes, with typical values of S = 35 and $\delta^{18}O$ = 0.3‰[Refs. 119,120]). It is common practice to use these, or similar, parameters (and where needed also additional water-based hydrogen isotope data[119]) in straightforward end-member mass-balance calculations[e.g., 119–122]. We use such a calculation to consider the amount of Greenland melt-water addition (and, thus, ice-sheet mass loss) needed to cause a −1.3‰ amplitude change in seawater $\delta^{18}O$ at Eirik Drift, as found in core MD03-2664. This amount is equal to the difference between the fraction of Greenland melt before (f_{G0}) and after (f_{G1}) the change. All other terms are kept constant, to enable comparison of the effects due to Greenland melt-water change. We then find:

$$f_{G0} = \frac{\delta_{EGC} - [f_M\delta_M + f_S(\delta_{EGC} + 2.1) + f_A\delta_A]}{\delta_G}$$

$$f_{G1} = \frac{(\delta_{EGC} - 1.3) - [f_M\delta_M + f_S(\delta_{EGC} - 1.3 + 2.1) + f_A\delta_A]}{\delta_G}$$

Here, f is the mixing fraction, δ is the component-water $\delta^{18}O$, EGC indicates the East Greenland Current, M is for meteoric water, S indicates sea ice, A is for advected ocean water, and G is for Greenland melt water. We set the calculation up with modern values f_M = 0.005, f_S = 0.028, f_A = 0.93, and δ_{EGC} = −1‰ (Cox, 2010[Ref.119], p.98). As mentioned above, we kept these values constant in both cases. We thus find that f_{G0} = 0.041, while f_{G1} = 0.083. Using a salinity mass balance and a 5 × 10^6 m^3 per second mass flux of the EGC to calculate mass fluxes, the change in mixing fraction then implies 1.311 × 10^{-3} m per year of additional global sea-level addition due to Greenland melt-water input for the full −1.3‰ seawater $\delta^{18}O$ amplitude shift at Eirik Drift (using a world ocean surface area of 361.9 × 10^{12} m^2).

The full amplitude shift developed over ~6,000 years. However, it did not develop instaneously: the record shows that it developed in a somewhat sigmoidal manner, and if we approximate this with a linear growth rate, then the sea-level contribution determined from the seawater $\delta^{18}O$ change over the full 6,000 years comes to (0.5 × 6,000 × 1.311 × 10^{-3}) = 3.93 m. Therefore, we find that the median estimate for development of the observed Eirik Drift $\delta^{18}O_{sw}$ shift of −1.3‰ is about 4 m sea-level equivalent of melt-water input from Greenland. Propagation of generous (Gaussian) uncertainties in all parameters in this calculation, using a method similar to Rohling (2000)[Ref. 123], indicates that 1σ = 1.15 m. We conclude that both temporal structure and amplitude of the Eirik Drift sea-water $\delta^{18}O$ record support the Yau et al. (2016) reconstruction of Greenland ice-mass loss[124].

Supplementary Note 4.

Glacio-isostatic assessment of LIG sea-level records

Changes in mass loading at Earth's surface, due to ice-sheet growth and melt and consequent ocean-basin unloading and loading, results in a non-uniform sea-level pattern on a global scale. This is known as glacial isostatic adjustment (GIA). We have previously shown that millennial-scale relative sea level (RSL) fluctuations at Hanish Sill (Red Sea) are proxies for global mean sea-level (GMSL) fluctuations across glacial cycles, although there is a longer-term secular offset between absolute RSL and GMSL values[106,125]. These investigations described an envelope of RSL behaviours at Hanish Sill related to a range of parameters for Earth's viscous response. Other work has demonstrated that modelling of past sea level must account for ice-volume changes both prior to the period of interest, and subsequent to it. To model RSL during the LIG, therefore, at least 3 glacial cycles must be considered prior to the LIG[Ref.126]. The modelling must also consider the impact of different geographical ice-mass distributions, particularly during the preceding penultimate glacial maximum (PGM, marine isotope stage MIS 6)[50,107,126].

To use the continuously sampled Red Sea RSL curves to constrain the volume of polar ice melt during the LIG, we must understand how these RSL curves are affected by GIA. If the GIA signal can be isolated using the models, then it can be removed from the RSL records to recover GMSL. Where that GMSL varies from the present-day 0 m level, the offset may then be interpreted in terms of excess ice-volume melt (or growth). Note, however, that this is complicated by the fact that 'excess ice' will impose a fingerprint of GIA response. To address this, Hay et al. (2014)[Ref.127] sought to highlight those regions where a highstand identified in proxy RSL indicators would overstate GMSL at a given point in time. In their scenario for coincident Greenland and Antarctic melt, Hanish Sill fell outside of these regions. When considering the impact of melt from individual ice sheets, Antarctic melt marginally amplified Red Sea RSL highstands, whereas Greenland melt caused a minor reduction in RSL highstands.

We extend previous GIA modelling to consider:

1) a LIG of ~14 ka duration (130-116 ka) with ice volumes held at present-day values to identify a background GIA signal;
2) four ice scenarios representing variations in both melt volume and geographic ice-mass distribution;
3) a broad suite of Earth models, highlighting results from four models that illustrate the influence of Earth-model choice on reconstructions; and
4) sensitivity tests that—across the above scenarios—analyse the consequences of 'excess ice' reduction or growth on Hanish Sill responses to individual ice-sheet changes.

For the GIA modelling we use a gravitationally self-consistent sea-level theory[128], which accounts for shoreline migration associated with local sea-level variations and changes in the extent of grounded, marine-based ice. The theory incorporates perturbations of Earth's rotation[129] resulting from changing ice-melt or -growth locations. The sea-level equation is solved in an iterative, pseudo-spectral manner[130] with a 1-D spherically symmetric Earth representation. In total, we model responses across a suite of 495 Earth models comprising 3 parameters for lithosphere thickness (71, 96, and 120 km), 11 parameters for upper

mantle viscosity (1×10^{20} to 1×10^{21} Pa s), and 15 parameters for lower mantle viscosity (2×10^{21} to 5×10^{22} Pa s). From these, we highlight four Earth models to display a range of behaviours (*Supplementary Table* 1). Our first three Earth models are similar to those used by Stocchi et al. (2018)[Ref.131]. Our fourth Earth model is chosen to highlight non-standard outlier (<4%) behaviour.

Supplementary Table 1. Earth model parameters used in our glacio-isostatic adjustment modelling.

Earth model	Upper mantle viscosity × 10^{21} Pa s	Lower mantle viscosity × 10^{21} Pa s	Rationale for this Earth model
EM1	1	2	Like VM1
EM2	0.5	5	Like VM2
EM3	0.25	0.1	Lambeck et al. (2014)[Ref.132] (similar to Hay et al. (2014)[Ref.127])
EM4	1	0.5	Extreme outlier for maximum contrast

We investigate RSL behaviour at Hanish Sill during the LIG using the four ice histories developed to investigate sea-level/ice-volume differences between the LGM and PGM[Ref.107]. All four ice histories model ice-volume changes at 2 kyr intervals between 244 ka and present day. Each contains a LIG period between 130 and 116 ka with present-day ice volume. ICE-1 is a version of the ICE-5G ice history[133], and covers two identical glacial cycles. The other three scenarios build on, or adjust, this basic ice history[104]. ICE-2 contains reduced ice volume during the PGM relative to the LGM. ICE-3 also has redistributed ice masses, giving a smaller North American ice sheet, and a larger European ice sheet during the PGM than during the LGM. ICE-4 also has different geographic boundaries for the European ice sheet, after de Boer et al. (2014)[134], while retaining the same ice-volume as ICE-2 and ICE-3.

We find that, when LIG ice volume is held constant, the Hanish Sill RSL response is generally characterised, irrespective of ice history, by an early highstand at the beginning of the interglacial and a subsequent decay toward equilibrium RSL (*Supplementary Figure 5*). For ICE-1 and ICE-2, the initial highstand is higher than GMSL, whereas for ICE-3 and ICE-4 both the initial highstand and the subsequent decay fall below GMSL. Importantly, we note that the total amplitude of this variation across the LIG is only a few metres, and so cannot account for the variations of 10 or more metres observed in our study (Figure 2, main text). For a small outlier subgroup (<4%) of the Earth models investigated, and only for ICE-3 and ICE-4, the viscosity contrast between upper and lower mantle values is such that a highstand is only achieved at the end of the interglacial. We illustrate this outlier behaviour with our fourth Earth model, but note that existing studies focus on EM1-3, as below.

Our main experiments considered only a 'background' interglacial scenario with no ice melt or growth greater than present day. To assess sensitivity to 'excess ice' variations, we therefore also modelled the responses at Hanish Sill for each individual ice sheet on its own, for individual ice-sheet configurations (*Supplementary Figure 6*). In *Supplementary Figure 6*, configuration A is for an ICE-5G like distribution of ice volume during MIS 6, and configuration B follows an ice-distribution template based on de Boer et al. (2014)[Ref.134]. Responses to Greenland and Antarctic ice-volume changes are similar. The 1:1 line in the graphs indicates no GIA effect, while values below the line indicate that the RSL response is an amplification of the GMSL change (i.e., RSL is higher than GMSL) and values above the line

represent points where RSL is lower than GMSL. For melt associated with the Greenland ice sheet, there is relatively little Earth model sensitivity – the points all cluster tightly along the same line, and generally fall close to the 1:1 line. The impact of Antarctic ice-volume change is highly dependent on the Earth model chosen, but overall such impacts plot along the 1:1 line, which suggests that RSL changes also closely approximate GMSL changes for Antarctic ice-volume changes.

Given that ice scenarios ICE-3 and ICE-4 are considered to be more representative of actual PGM ice-volume distributions[107], and therefore to generate results closer to reality, we infer that the LIG RSL generated for Hanish Sill likely underestimates GMSL by a few metres in absolute terms (slightly more in the later phases than in the beginning). Given this, and the minimal GIA effects that we find at Hanish Sill for Antarctic ice-mass reduction, we consider RSL fluctuations in the first half of the LIG (Figure 2, main text) to be close approximations of GMSL fluctuations. For the second half of the LIG, where ice-mass reduction is considered to have occurred at both Greenland and Antarctica (Figure 3, main text), offsets are again small, and we consider that Red Sea RSL fluctuations again closely approximate GMSL fluctuations.

Where we make GIA corrections to approximately translate Red Sea RSL into GMSL, we use a linear adjustment for the RSL gradient through the LIG from +0 ±0 m at 135 ka, to +4 ±2 m at 115 ka, based on the ICE3 and ICE4 solutions for the three representative EMs 1-3 (*Supplementary Figure 5*). Note that the uncertainties here refer to the gradient through the LIG, not to absolute values.

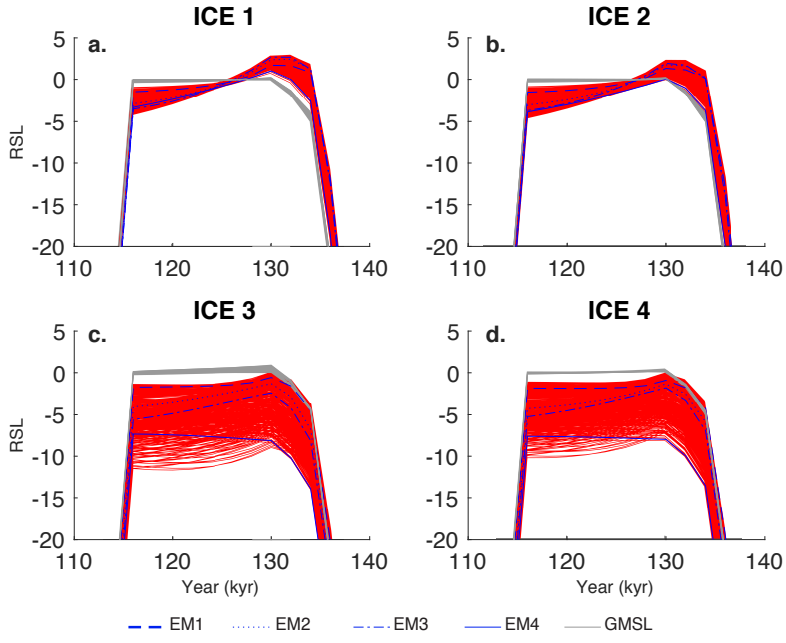

Supplementary Figure 5. Red Sea relative sea level (RSL) *versus* global mean sea level (GMSL) for 495 Earth models at the Hanish Sill, and ice scenarios ICE 1-4. Red lines for all four graphs represent RSL for the full suite of 495 Earth models (EMs) considered. Blue lines represent the four highlighted EMs, and grey lines represent GMSL. **A and B.** For these ice histories RSL tends to overshoot GMSL at the beginning of the interglacial and then decay to an equilibrium value. **C and D.** A greater range in RSL values results from sensitivity to a larger PGM Eurasian ice sheet. Note also the EM sensitivity, where EM1-3 represent the majority in which a highstand occurs at the beginning of the LIG, while EM4 represents an outlier group (<4%) in which the highstand occurs at the end of the LIG.

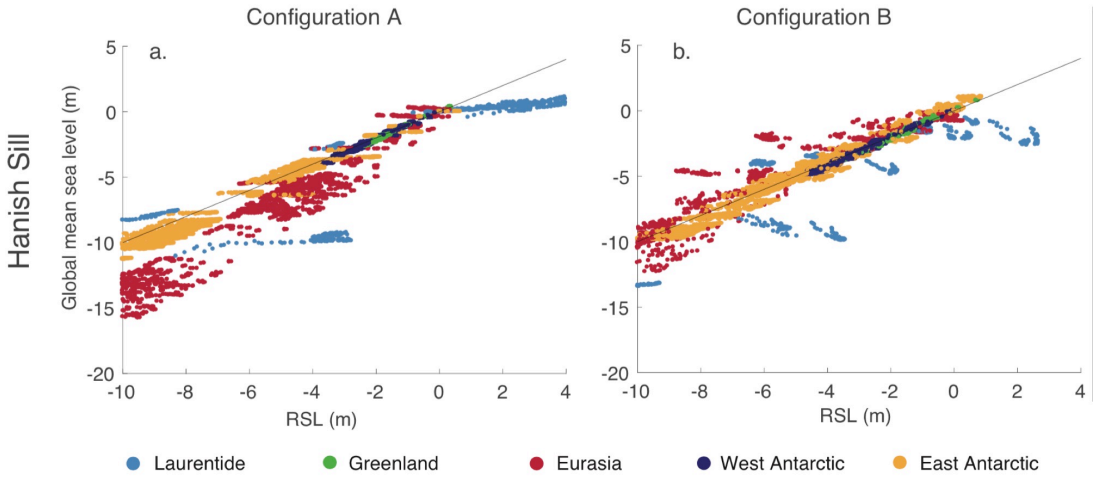

Supplementary Figure 6. Hanish Sill relative sea level (RSL) *versus* global mean sea level (GMSL) for a representative subset of 60 Earth models from our total suite of 495 Earth models. Results are obtained from runs of our GIA model in which individual ice sheets are isolated based on two synthetic ice histories (configuration **A** relies on the ice distribution in ICE-5G, and configuration **B** on that of de Boer et al. (2014)[Ref.134]. The plotted RSL and GMSL signals then represent only the GIA signal associated with the selected individual ice sheet (blue represents North American ice sheets, green represents Greenland, red represents Eurasian ice sheets, and navy and gold represent the West and East Antarctic ice sheets, respectively). Relatively wide horizontal dispersal of red data points indicates considerable sensitivity to EM choice for Eurasian ice sheet responses. In contrast, Antarctic ice-sheet responses (navy and gold) are horizontally tightly clustered, indicating little influence of EM choice. In addition, both Antarctic datapoints (esp. West Antarctica), and Greenland datapoints plot close to the black 1:1 line, which indicates minimal GIA effects at Hanish Sill in response to mass changes in those ice sheets.

Supplementary Note 5.

Consistency between Red Sea and coral-based sea-level reconstructions

Given the dynamic nature of the Red Sea sea-level curve through the LIG, it is difficult to visualise the type of coral record with which this would be consistent. Therefore, we have developed a straightforward model for first-order evaluation. We assume that the Red Sea sea-level record is representative of sea-level movements through the LIG (using the PM solution in this example), following a simple approximate correction for GIA effects (see section 4). For the latter, we use the ICE3 and ICE4 solutions for the three representative EMs, and approximate these by a linear RSL adjustment by +0 m at 135 ka to +4 m at 115 ka, to obtain roughly approximated GMSL values (*Supplementary Figure 7*). These rough adjustments are sufficient because we are concerned with a basic consistency test only.

In essence, we approximate fringing-reef development by assuming total occupation of available accommodation space by reef growth, subject to certain limitations. First, it is assumed that accommodation space for coral growth has an upper depth limit at –1 m water depth, to represent Mean Low Tide over an array of regions, from microtidal regions to regions with large tidal ranges. The chosen value does not affect our conclusions; changes merely shift the simulated reef records up and down in absolute terms. Second, it is assumed that reef-growth rate is optimal over the first 20 m below the upper depth limit, and that it then linearly tapers to zero at about 100 m depth. Third, the model explores two variables:

(a) the influence of reef tolerance to drowning due to rapid sea-level rise; (b) the inverse, namely reef tolerance to rapid sea-level lowering.

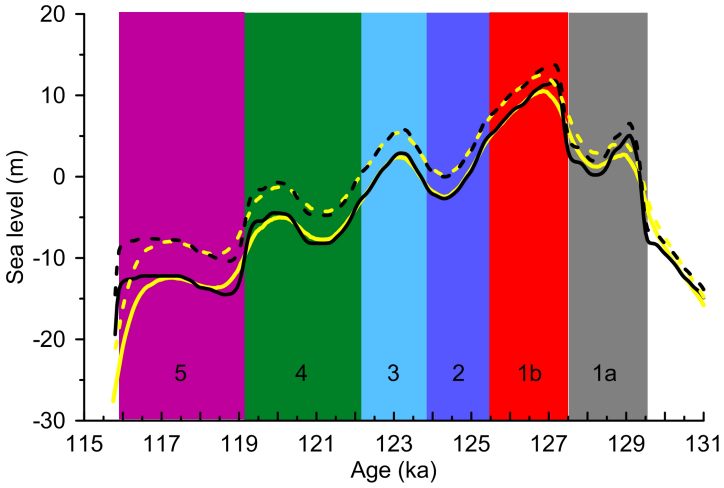

Supplementary Figure 7. Identification of reef-growth phases portrayed in Supplementary Figure 8. Solid lines portray PM (black) and Median (yellow) of the probabilistic Red Sea RSL analysis (Figure 2g). Dashed lines portray PM (black) and Median (yellow) as above, but after schematic GIA correction to rough GMSL values based on linear approximation between 0 m adjustment at 135 ka, and 5 m adjustment at 115 ka. Colours and numbers refer to reef accretion phases in *Supplementary Figure 8*.

The experiments (*Supplementary Figure 8*) start with a sea floor of arbitrary slope. The vertical axis is specified in metres, and the arbitrary slope determines an arbitrary horizontal axis (coastal/shelf width). The chosen slope does not change the modelled pattern of reef formation; it only compresses (steeper slopes) or widens (shallower slopes) the reconstructions laterally. When the simulated sea floor falls within the upper zone of optimal growth, the model allows a reef to fill the entire accommodation space to the limiting depth of –1 m, except when the sea-level lowering or rise thresholds are exceeded, in which case growth is halted. Results over a wide range of specified sea-level lowering threshold values indicate that this parameter has no appreciable impacts so it is ignored hereafter. In contrast, the tolerance threshold value for sea-level rise is critically important.

When sea-level rise exceeds the specified tolerance threshold value, the reef "drowns" and growth is halted in the model until sea-level rise returns below the threshold again. Although coral populations have evolved through the Plio-Pleistocene to cope with rapid sea-level fluctuations[135], threshold values for “keeping up” *versus* “drowning” still vary per taxon. Fast-growing taxa include *Acropora* and *Pocillopora*, while slow-growing corals include *Porites* and faviids[136]. Slow growers have typical growth rates of 10-20 mm/y and fast growers can reach 40-100 mm/y[Refs.136,137]. Individual species growth rates (and hence the dominant assemblages) have an impact on reef accretion rates, and typically reef accretion rates are around 4 mm/y (range: 1-9 mm/y, or 0.4 $^{+0.5}/_{-0.3}$ m per century, m/c)[138,139], with very high values up to 26 mm/y or 2.6 m/c[Ref.138] and only in exceptional cases reaching 30 mm/y or more (3 m/c[Refs.86,140]). Higher values can be accommodated only by landward stepping of reef growth, e.g., the ~5 m/c of melt-water pulse 1a, at around 14.5 ka[Ref.86]. To bracket all options, we explore values from 0.5 m/c to 6 m/c.

The expected reef expression for different modelled LIG phases varies considerably as a function of the specified value of tolerance to “drowning” due to sea-level rise (*Supplementary* Figure 8). It is especially striking that reefs with exceptional drowning tolerances (thresholds ⩾3 m/c; Supplementary Figure 8e-h) are needed to obtain significant expressions of the highest peak (Phase 1b; *Supplementary Figures* 7 and 8). Even higher tolerances (⩾4 m/c; *Supplementary Figure 8f-h*) are needed before that peak would develop

strong expressions. In areas with reef assemblages with tolerances within the observed range (<3m/c), Phase 1b would be hardly developed, if at all (*Supplementary Figure 8a-d*).

Over the range of the most common tolerance levels (0.5 to 2 m/c), the model suggests that most LIG reef deposits should be expected to occur between –2 and +5 m, relative to GMSL, with negligible expression of rapid sea-level variability (*Supplementary Figure 8a-c*), which is reasonably consistent with reported observations (*Supplementary Figure 9*). We, therefore, contend that absence of reef deposits at higher elevations does not imply inconsistency with the Red Sea-based sea-level target curve used here.

Note that our simple exercise reports all results relative to GMSL. It is possible that local GIA and/or tectonic movements relative to GMSL created exceptional "windows" that allowed preservation of Phase 1b expressions even in regions that have reef assemblages with drowning tolerances <3 m/c. Essentially, vertical ground movement (uplift) would in those cases (partially) offset rapid sea-level rise to a sufficient degree to prevent reef drowning. We suggest that more elaborate/realistic predictive modelling along with GIA and tectonic assessment may in future provide clues to identify the most promising (especially uplifting) locations for recovering Phase 1b.

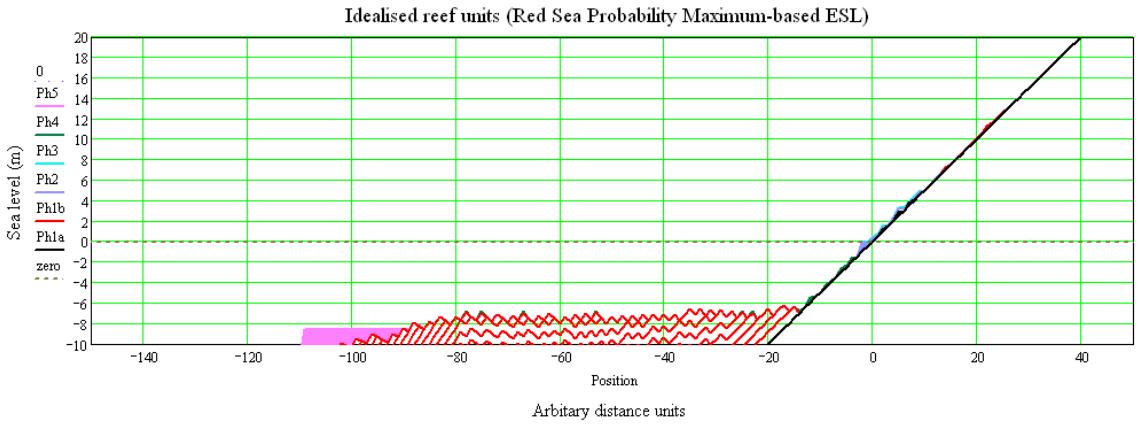

a.

0.5 m/c

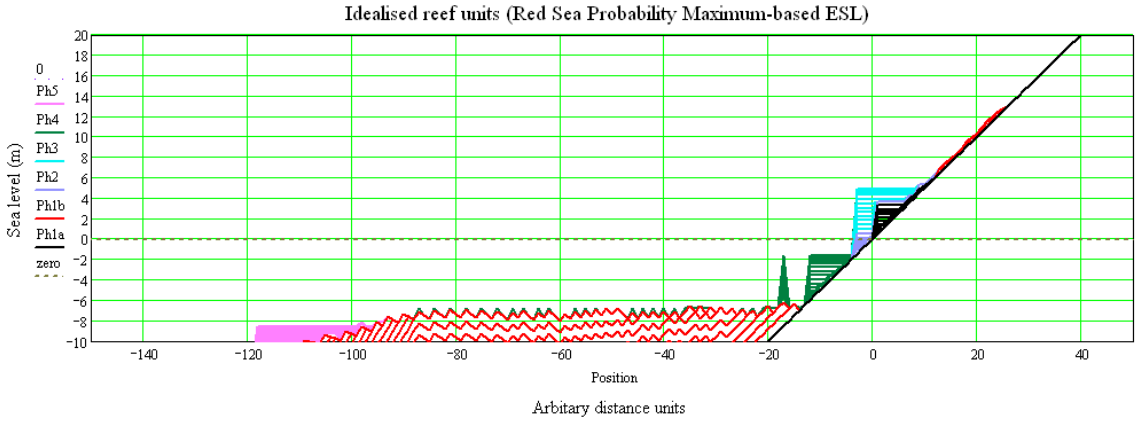

b.

1.0 m/c

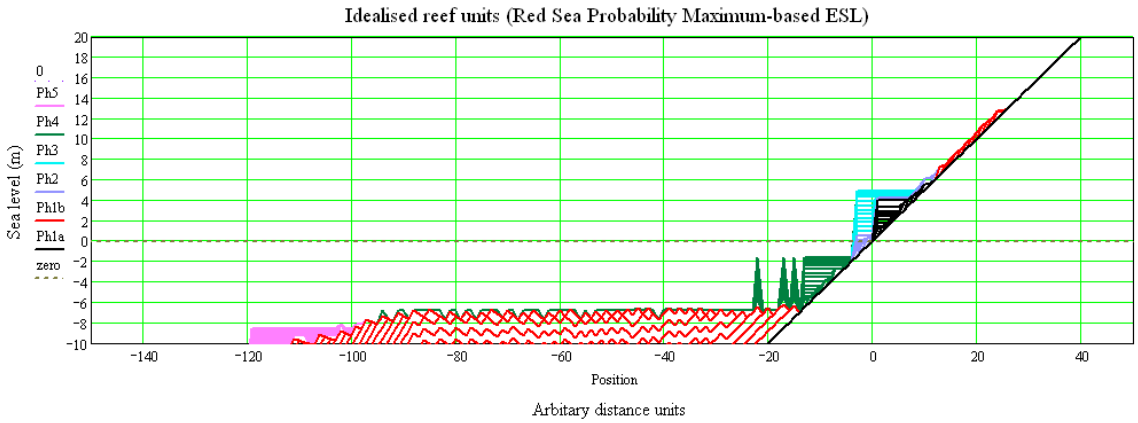

c.

1.5 m/c

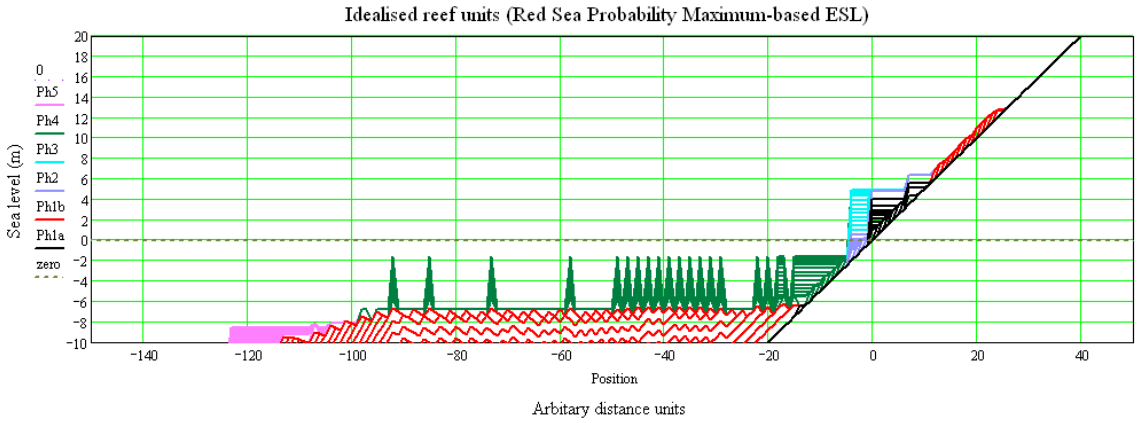

d.

2.0 m/c

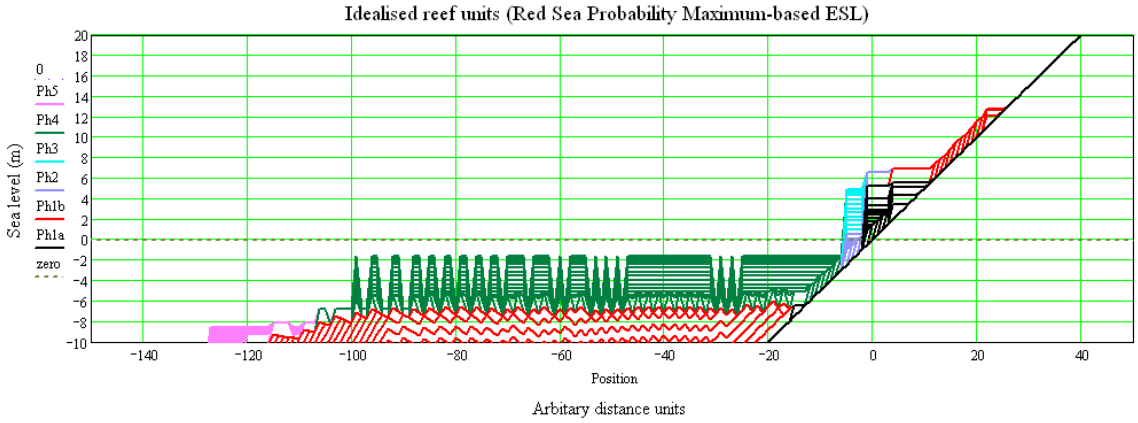

e.

3.0 m/c

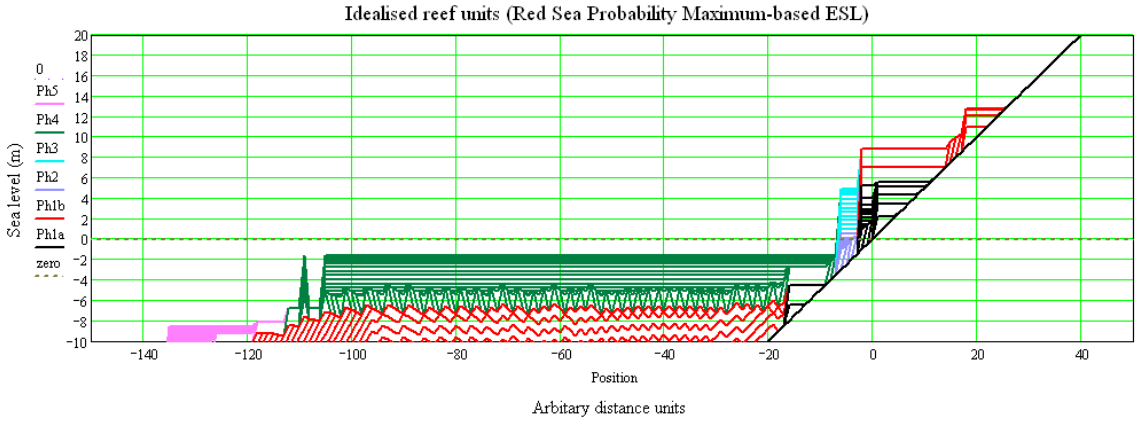

f.

4.0 m/c

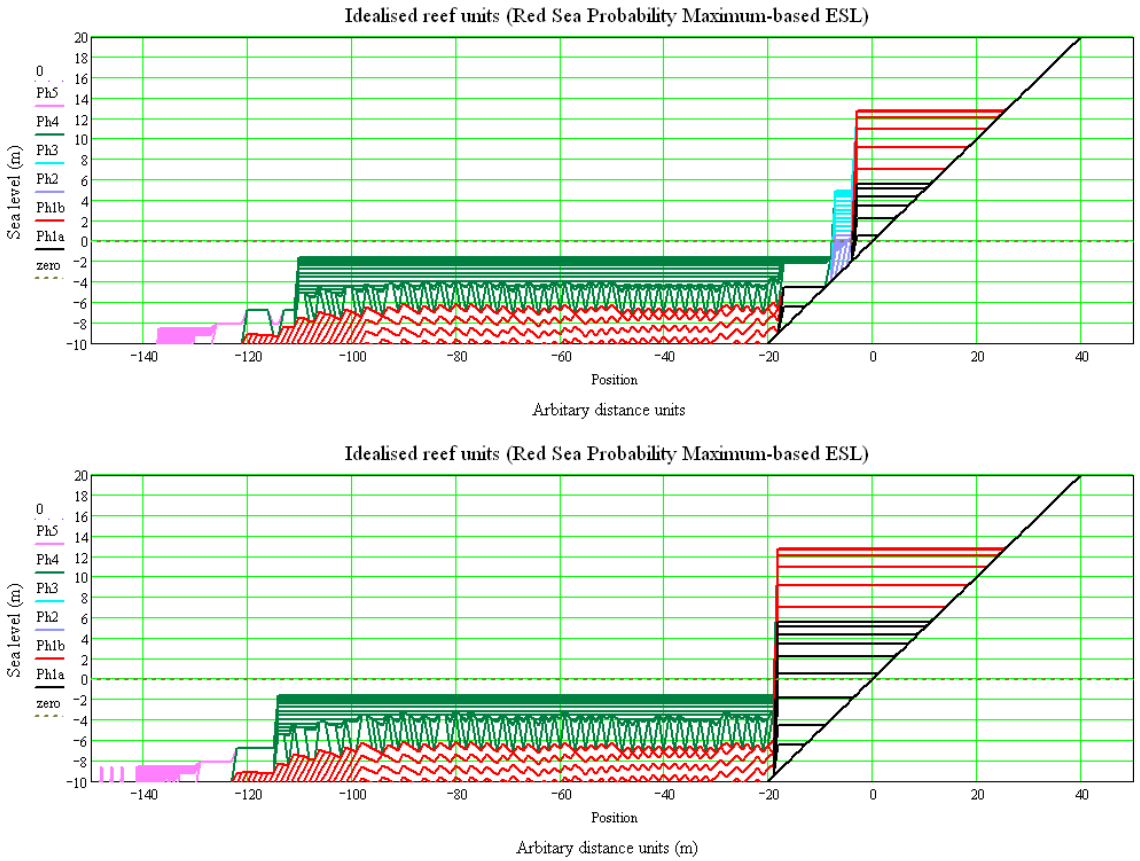

g.

5.0 m/c

h.

6.0 m/c

Supplementary Figure 8. Idealised modelled reef units for a schematic Red Sea probability maximum-based global mean sea level (GMSL) reconstruction. Successive panels (**a**-**h**) represent model results for different specified reef "drowning" tolerance threshold values (in terms of rate of sea-level rise), as indicated on the right-hand side. Colours identify different LIG reef phases, as per *Supplementary* Figure 7.

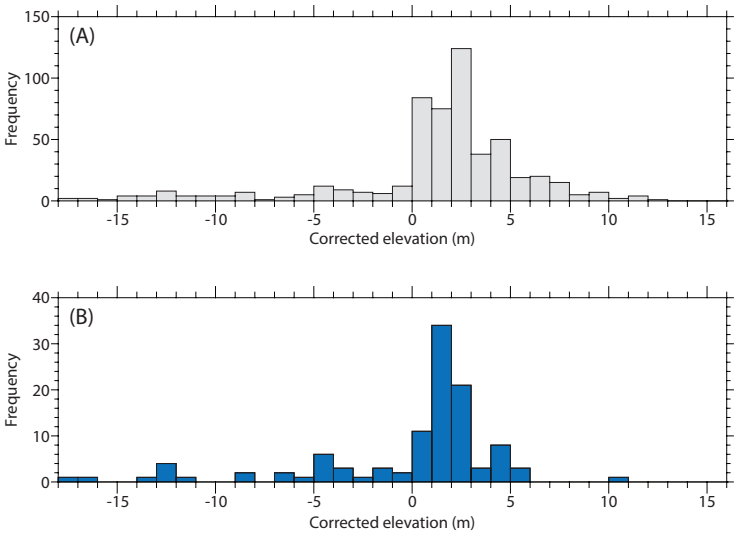

Supplementary Figure 9. Histograms of Last Interglacial coral elevations corrected for tectonic uplift or subsidence since the time of formation (from the compilation of Ref.[87]). **A.** All corals of LIG age[1,8,9,13,17,21,22,26,28-30,37,66–72,76,79,83–90,120–143] (grey). **B.** Subset from A that fulfils age reliability screening criteria (blue) (calcite <2%, ^{232}Th concentration < 2 ppb and $\delta^{234}U_{initial}$ = 147 ± 5 ‰)[8,9,75,79,102,109–114,143,13,147,15,25,29,69–71,73].

Supplementary Note 6.

Rates of sea-level drop between sea-level rise events during the LIG

We acknowledges that it is not yet fully possible to reconcile the high rates of sea-level variability observed in geological archives with current understanding of ice physics. High rates of sea-level rise may be explained through dynamic processes of ice-mass loss that are underestimated[e.g.,167,168]. However, high rates of sea-level lowering require high rates of ice-mass growth, and are less easy to explain. In our Red Sea reconstructions, translated to GMSL as explained in sections 4 and 5, rates of sea-level change are less than –1 m/c for all lowering events bar one (at ~119.1 ka in the $GMSL_{PM}$ reconstruction; i.e., that based on the calculated probability maximum) (*Supplementary Figure 10*). Moreover, average sea-level drop values across entire intervals of sea-level lowering range between –0.23 and –0.63 m/c.

We can consider these values in a rough ball-park assessment. Gross ice accumulation over Greenland and Antarctica is determined by snowfall. This precipitation is not likely to stop because it depends on moisture availability (evaporation) and active weather systems. Gross accumulation over Antarctica today is equivalent to about –0.6 m/c sea-level change[169], and for Greenland about –0.16 m/c sea-level change[170]. Thus, the present sea-level drop at no mass loss would be about –0.76 m/c sea-level change. Yet, the zero mass-loss criterion is unrealistic because melt and calving cannot be expected to be entirely zero. Still the value is considerably larger than the average sea-level drop values we infer across entire intervals of sea-level lowering (–0.23 to –0.63 m/c), while significant warming around Antarctica[171] and reduced sea-ice cover[172] would allow substantially increased moisture supply. This seems to be supported by a 30% accumulation rate increase, from ~30 to ~39 kg m^{-1} y^{-1} at EPICA Dome C[ref.173]. We also note that LIG mass loss is considered to have differed from the present in that fast ice-volume reduction phases led to isostatic rebound with resultant ice-shelf re-grounding, which then may have limited mass loss[174–178].

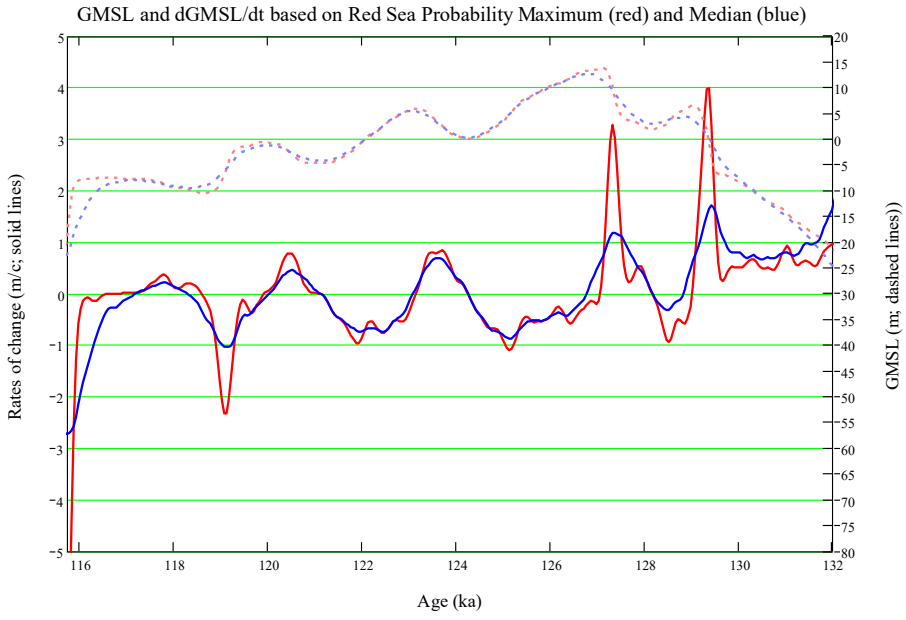

Supplementary Figure 10. Global mean sea level (GMSL, see *Supplementary Figure* 5) based on the Red Sea probability maxima (PM) and median reconstructions (red and blue dashed lines, respectively), along with their rates of change (solid). Data density for KL11 alone is too low <116 ka for robust results.

Supplementary References

1. Walter, R. C. *et al.* Early human occupation of the Red Sea coast of Eritrea during the last interglacial. *Nature* **405**, 65–69 (2000).
2. Bruggemann, H. J. *et al.* Stratigraphy, palaeoenvironments and model for the deposition of the Abdur Reef Limestone: context for an important archaeological site from the last interglacial on the Red Sea coast of Eritrea. *Palaeogeogr. Palaeoclimatol. Palaeoecol.* **203**, 179–206 (2004).
3. Plaziat, J.-C., Reyss, J.-L., Choukri, A. & Cazala, C. Diagenetic rejuvenation of raised coral reefs and precision of dating. The contribution of the Red Sea reefs to the question of reliability of the Uranium-series datings of middle to late Pleistocene key reef-terraces of the world. *Carnets Géologie / Notebooks Geol.* **4**, 2008/04 (2008).
4. Plaziat, J.-C. *et al.* Mise en evidence, sur la cote recifale d'Egypte, d'une regression interrompant brievement le plus haut niveau du dernier interglaciaire (5e); un nouvel indice de variations glacio-eustatiques a haute frequence au Pleistocene? *Bull. la Société Géologique Fr.* **169**, 115–125 (1998).
5. Plaziat, J.-C. *et al.* Quateranry changes in the Egyptian shoreline of the northwestern Red Sea and the Gulf of Suez. *Quat. Int.* **29/30**, 11–22 (1995).
6. Bar, N. *et al.* Last interglacial sea levels and regional tectonics from fossil coral reefs in the northeast Gulf of Aqaba. *Quat. Sci. Rev.* **191**, 41–56 (2018).
7. Yehudai, M. *et al.* U–Th dating of calcite corals from the Gulf of Aqaba. *Geochim. Cosmochim. Acta* **198**, 285–298 (2017).
8. Israelson, C. & Wohlfarth, B. Timing of the Last-Interglacial high sea level on the Seychelles Islands, Indian Ocean. *Quat. Res.* **51**, 306–316 (1999).
9. Dutton, A., Webster, J. M., Zwartz, D., Lambeck, K. & Wohlfarth, B. Tropical tales of polar ice: evidence of Last Interglacial polar ice sheet retreat recorded by fossil reefs of the granitic Seychelles islands. *Quat. Sci. Rev.* **107**, 182–196 (2015).
10. Vyverberg, K. *et al.* Episodic reef growth in the granitic Seychelles during the Last Interglacial: Implications for polar ice sheet dynamics. *Mar. Geol.* **399**, 170–187 (2018).
11. Chappell, J. Geology of coral terraces, Huon Peninsula, New Guinea: A study of Quaternary tectonic movements and sea-Level changes. *Geol. Soc. Am. Bull.* **85**, 553–570 (1974).
12. Chappell, J. & Veeh, H. H. Late Quaternary tectonic movements and sea-level changes at Timor and Atauro Island. *Geol. Soc. Am. Bull.* **89**, 356–368 (1978).
13. Stein, M. *et al.* TIMS U-series dating and stable isotopes of the last interglacial event in Papua New Guinea. *Geochim. Cosmochim. Acta* **57**, 2541–2554 (1993).
14. Aharon, P., Chappell, J. & Compston, W. Stable isotope and sea-level data from New Guinea supports Antarctic ice-surge theory of ice ages. *Nature* **283**, 649–651 (1980).
15. Chen, J. H., Curran, H. A., White, B. & Wasserburg, G. J. Precise chronology of the last interglacial period: ^{234}U-^{230}Th data from fossil coral reefs in the Bahamas. *Geol. Soc. Am. Bull.* **103**, 82–97 (1991).
16. White, B., Curran, H. A. & Wilson, M. A. Bahamian coral reefs yield evidence of a brief sea-level lowstand during the last interglacial. *Carbonates and Evaporites* **13**, 10–22 (1998).
17. Wilson, M. A., Curran, H. A. & White, B. Paleontological evidence of a brief global sea-level event during the last interglacial. *Lethaia* **31**, 241–250 (1998).
18. Hearty, P. J., Hollin, J. T., Neumann, A. C., O'Leary, M. J. & McCulloch, M. T. Global sea-level fluctuations during the Last Interglaciation (MIS 5e). *Quat. Sci. Rev.* **26**, 2090–2112 (2007).
19. Thompson, W. G., Curran, H. A., Wilson, M. A. & White, B. Sea-level oscillations during the last interglacial highstand recorded by Bahamas corals. *Nat. Geosci.* **4**, 684–687 (2011).
20. Skrivanek, A., Li, J. & Dutton, A. Relative sea-level change during the Last Interglacial as recorded in Bahamian fossil reefs. *Quat. Sci. Rev.* **200**, 160–177 (2018).
21. Kerans, C., Zahm, C., Bachtel, S. L., Hearty, P. & Cheng, H. Anatomy of a late Quaternary carbonate island: Constraints on timing and magnitude of sea-level fluctuations, West Caicos, Turks and Caicos Islands, BWI. *Quat. Sci. Rev.* **205**, 193–223 (2019).
22. Neumann, A. C. & Hearty, P. J. Rapid sea-level changes at the close of the last interglacial

(substage 5e) recorded in Bahamian island geology. *Geology* **24**, 775–778 (1996).
23. Hearty, P. J. & Kindler, P. Sea-Level highstand chronology from stable carbonate platforms (Bermuda and the Bahamas). *J. Coast. Res.* **11**, 675–689 (1995).
24. Hearty, P. J. & Neumann, A. C. Rapid sea level and climate change at the close of the Last Interglaciation (MIS 5e): evidence from the Bahama Islands. *Quat. Sci. Rev.* **20**, 1881–1895 (2001).
25. Blanchon, P., Eisenhauer, A., Fietzke, J. & Liebetrau, V. Rapid sea-level rise and reef back-stepping at the close of the last interglacial highstand. *Nature* **458**, 881–884 (2009).
26. Harmon, R. S. *et al.* U-series and amino-acid racemization geochronology of Bermuda: implications for eustatic sea-level fluctuation over the past 250,000 years. *Palaeogeogr. Palaeoclimatol. Palaeoecol.* **44**, 41–70 (1983).
27. Rowe, M. P., Wainer, K. A. I., Bristow, C. S. & Thomas, A. L. Anomalous MIS 7 sea level recorded on Bermuda. *Quat. Sci. Rev.* **90**, 47–59 (2014).
28. Hearty, P. J. & Tormey, B. R. Sea-level change and superstorms; geologic evidence from the last interglacial (MIS 5e) in the Bahamas and Bermuda offers ominous prospects for a warming Earth. *Mar. Geol.* **390**, 347–365 (2017).
29. Muhs, D. R., Simmons, K. R. & Steinke, B. Timing and warmth of the Last Interglacial period: new U-series evidence from Hawaii and Bermuda and a new fossil compilation for North America. *Quat. Sci. Rev.* **21**, 1355–1383 (2002).
30. Hearty, P. J. Revision of the Late Pleistocene stratigraphy of Bermuda. *Sediment. Geol.* **153**, 1–21 (2002).
31. Muhs, D. R., Simmons, K. R., Schumann, R. R. & Halley, R. B. Sea-level history of the past two interglacial periods: new evidence from U-series dating of reef corals from south Florida. *Quat. Sci. Rev.* **30**, 570–590 (2011).
32. Fruijtier, C., Elliott, T. & Schlager, W. Mass-spectrometric ^{234}U-^{230}Th ages from the Key Largo Formation, Florida Keys, United States: Constraints on diagenetic age disturbance. *Geol. Soc. Am. Bull.* **112**, 267–277 (2000).
33. Halley, R. B. & Evans, C. *The Miami Limestone: a guide to selected outcrops and their interpretation*. (1983).
34. Sherman, C. E., Glenn, C. R., Jones, A. T., Burnett, W. C. & Schwarcz, H. P. New evidence for two highstands of the sea during the last interglacial, oxygen isotope substage 5e. *Geology* **21**, 1079–1082 (1993).
35. Ku, T., Kimmel, M. A., Easton, W. H. & O'Neil, T. J. Eustatic Sea Level 120,000 Years Ago on Oahu, Hawaii. *Science (80-.).* **183**, 959–962 (1974).
36. Muhs, D. R. & Szabo, B. J. New uranium-series ages of the Waimanalo Limestone, Oahu, Hawaii: Implications for sea level during the last interglacial period. *Mar. Geol.* **118**, 315–326 (1994).
37. Stearns, H. T. Quaternary shorelines in the Hawai'ian Islands. *B.P. Bish. Museum Bull.* **237**, 1–57 (1978).
38. Hearty, P. J., Kaufman, D. S., Olson, S. L. & James, H. F. Stratigraphy and whole-rock amino acid geochronology of key Holocene and Last Interglacial carbonate deposits in the Hawaiian Islands. *Pacific Sci.* **54**, 423–442 (2000).
39. Szabo, B. J., Ludwig, K. R., Muhs, D. R. & Simmons, K. R. Thorium-230 ages of corals and duration of te Last Interglacial sea-level high stand on Oahu, Hawaii. *Science (80-.).* **266**, 93–96 (1994).
40. Johnson, M. E., Baarli, B. G. & Scott Jr., J. H. Colonization and reef growth on a Late Pleistocene rocky shore and abrasion platform in Western Australia. *Lethaia* **28**, 85–98 (1995).
41. Hearty, P. J. An inventory of last interglacial (*sensu lato*) age deposits from the Mediterranean Basin: a study of isoleucine epimerization and U-series dating. *Zeitschrift für Geomorphol.* **62**, 51–69 (1986).
42. Mauz, B., Fanelli, F., Elmejdoub, N. & Barbieri, R. Coastal response to climate change: Mediterranean shorelines during the Last Interglacial (MIS 5). *Quat. Sci. Rev.* **54**, 89–98 (2012).
43. Zazo, C. *et al.* Pleistocene raised marine terraces of the Spanish Mediterranean and Atlantic

coasts: records of coastal uplift, sea-level highstands and climate changes. *Mar. Geol.* **194**, 103–122 (2003).
44. Carobene, L. Marine notches and sea-cave bioerosional grooves in microtidal areas: examples from the Tyrrhenian and Ligurian Coasts - Italy. *J. Coast. Res.* **31**, 536–556 (2015).
45. Mauz, B. & Antonioli, F. Comment on "Sea level and climate changes during OIS 5e in the Western Mediterranean" by T. Bardají, J.L. Goy, J.L., C. Zazo, C. Hillaire-Marcel, C.J. Dabrio, A. Cabero, B. Ghaleb, P.G. Silva, J. Lario, Geomorphology 104 (2009), 22–37. *Geomorphology* **110**, 227–230 (2009).
46. Bardají, T. *et al.* Sea level and climate changes during OIS 5e in the Western Mediterranean. *Geomorphology* **104**, 22–37 (2009).
47. Ferranti, L. *et al.* Markers of the last interglacial sea-level high stand along the coast of Italy: Tectonic implications. *Quat. Int.* **145–146**, 30–54 (2006).
48. Muhs, D. R., Simmons, K. R., Meco, J. & Porat, N. Uranium-series ages of fossil corals from Mallorca, Spain: The "Neotyrrhenian" high stand of the Mediterranean Sea revisited. *Palaeogeogr. Palaeoclimatol. Palaeoecol.* **438**, 408–424 (2015).
49. Sisma-Ventura, G. *et al.* Last interglacial sea level high-stand deduced from well-preserved abrasive notches exposed on the Galilee coast of northern Israel. *Palaeogeogr. Palaeoclimatol. Palaeoecol.* **470**, 1–10 (2017).
50. Sivan, D. *et al.* Eastern Mediterranean sea levels through the last interglacial from a coastal-marine sequence in northern Israel. *Quat. Sci. Rev.* **145**, 204–225 (2016).
51. Antonioli, F., Ferranti, L. & Kershaw, S. A glacial isostatic adjustment origin for double MIS 5.5 and Holocene marine notches in the coastline of Italy. *Quat. Int.* **145–146**, 19–29 (2006).
52. Jedoui, Y. *et al.* U-series evidence for two high Last Interglacial sea levels in southeastern Tunisia. *Quat. Sci. Rev.* **22**, 343–351 (2003).
53. Mauz, B., Shen, Z., Elmejdoub, N. & Spada, G. No evidence from the eastern Mediterranean for a MIS 5e double peak sea-level highstand. *Quat. Res.* **89**, 505–510 (2018).
54. Chakroun, A., Zaghbib-Turki, D., Miskovsky, J.-C. & Davaud, E. Two Tyrrhenian transgressive cycles in coastal deposits of the Cap Bon Peninsula, Tunisia. *Quaternaire* **20**, 215–226 (2009).
55. Dabrio, C. J. *et al.* Millennial/submillennial-scale sea-level fluctuations in western Mediterranean during the second highstand of MIS 5e. *Quat. Sci. Rev.* **30**, 335–346 (2011).
56. Zazo, C. *et al.* Retracing the Quaternary history of sea-level changes in the Spanish Mediterranean–Atlantic coasts: Geomorphological and sedimentological approach. *Geomorphology* **196**, 36–49 (2013).
57. Hillaire-Marcel, C. *et al.* U-series measurements in Tyrrhenian deposits from Mallorca - Further evidence for two last-interglacial high sea levels in the Balearic Islands. *Quat. Sci. Rev.* **15**, 53–62 (1996).
58. Hillaire-Marcel, C., Carro, O., Causse, C., Goy, J. L. & Zazo, C. Th/U dating of Strombus bubonis-bearing marine terraces in southeastern Spain. *Geology* **14**, 613–616 (1986).
59. Zazo, C. *et al.* The Last Interglacial in the Mediterranean as a model for the present interglacial. *Glob. Planet. Change* **7**, 109–117 (1993).
60. Hearty, P. J., Hollin, J. T. & Dumas, B. Geochronology of Pleistocene littoral deposits on the Alicante and Almeria coasts of Spain. in *Cambios del nivel del mar en Espana en el Cuaternario reciente* **10**, 95–107 (1987).
61. Tuccimei, P. *et al.* Last interglacial sea level changes in Mallorca island (Western Mediterranean). High precision U-series data from phreatic overgrowths on speleothems. *Zeitschrift für Geomorphol.* **50**, 1–21 (2006).
62. Dorale, J. A. *et al.* Sea-Level Highstand 81,000 Years Ago in Mallorca. *Science (80-.).* **327**, 860–863 (2010).
63. Fornós, J. J. *et al.* Phreatic overgrowths on speleothems: a useful tool in structural geology in littoral karstic landscapes. The example of eastern Mallorca (Balearic Islands). *Geodin. Acta* **15**, 113–125 (2002).
64. Tuccimei, P. *et al.* Sea level change at Capo Cacia (NW Sardinia) and Mallorca (Balearic Islands) during oxygen isotope substage 5e, based on Th/U datings of phreatic overgrowths

on speleothems. *Monogr. Nat. Hist. Soc. Balear.* **14**, 121–135 (2007).
65. Muhs, D. R., Meco, J. & Simmons, K. R. Uranium-series ages of corals, sea level history, and palaeozoogeography, Canary Islands, Spain: An exploratory study for two Quaternary interglacial periods. *Palaeogeogr. Palaeoclimatol. Palaeoecol.* **394**, 99–118 (2014).
66. Blanchon, P. Reef demise and back-stepping during the last interglacial, northeast Yucatan. *Coral Reefs* **29**, 481–498 (2010).
67. Blanchon, P. & Shaw, J. Reef drowning during the last deglaciation: Evidence for catastrophic sea-level rise and ice-sheet collapse. *Geology* **23**, 4–8 (1995).
68. Blanchon, P., Jones, B. G. & Ford, D. C. Discovery of a submerged relic reef and shoreline off Grand Cayman: further support for an early Holocene jump in sea level. *Sediment. Geol.* **147**, 253–270 (2002).
69. Zhu, Z. R. *et al.* High-precision U-series dating of Last Interglacial events by mass spectrometry: Houtman Abrolhos Islands, western Australia. *Earth Planet. Sci. Lett.* **118**, 281–293 (1993).
70. Stirling, C. H., Esat, T. M., McCulloch, M. T. & Lambeck, K. High-precision U-series dating of corals from Western Australia and implications for the timing and duration of the Last Interglacial. *Earth Planet. Sci. Lett.* **135**, 115–130 (1995).
71. Stirling, C. H., Esat, T. M., Lambeck, K. & McCulloch, M. T. Timing and duration of the Last Interglacial: evidence for a restricted interval of widespread coral reef growth. *Earth Planet. Sci. Lett.* **160**, 745–762 (1998).
72. O'Leary, M. J., Hearty, P. J. & McCulloch, M. T. Geomorphic evidence of major sea-level fluctuations during marine isotope substage-5e, Cape Cuvier, Western Australia. *Geomorphology* **102**, 595–602 (2008).
73. O'Leary, M. J., Hearty, P. J. & McCulloch, M. T. U-series evidence for widespread reef development in Shark Bay during the last interglacial. *Palaeogeogr. Palaeoclimatol. Palaeoecol.* **259**, 424–435 (2008).
74. O'Leary, M. J. *et al.* Ice sheet collapse following a prolonged period of stable sea level during the last interglacial. *Nat. Geosci.* **6**, 796–800 (2013).
75. Eisenhauer, A., Zhu, Z. R., Collins, L. B., Wyrwoll, K. H. & Eichstätter, R. The Last Interglacial sea level change: new evidence from the Abrolhos islands, West Australia. *Geol. Rundschau* **85**, 606–614 (1996).
76. Whitney, B. B. & Hengesh, J. V. Geomorphological evidence of neotectonic deformation in the Carnarvon Basin, Western Australia. *Geomorphology* **228**, 579–596 (2015).
77. Dumas, B., Hoang, C. T. & Raffy, J. Record of MIS 5 sea-level highstands based on U/Th dated coral terraces of Haiti. *Quat. Int.* **145–146**, 106–118 (2006).
78. Dodge, R. E., Fairbanks, R. G., Benninger, L. K. & Maurrasse, F. Pleistocene sea levels from raised coral reefs of Haiti. *Science (80-.).* **219**, 1423–1425 (1983).
79. Blanchon, P. & Eisenhauer, A. Multi-stage reef development on Barbados during the Last Interglaciation. *Quat. Sci. Rev.* **20**, 1093–1112 (2001).
80. Thompson, W. G. & Goldstein, S. L. Open-system coral ages reveal persistent suborbital sea-level cycles. *Science (80-.).* **308**, 401–404 (2005).
81. Schellmann, G. & Radtke, U. A revised morpho- and chronostratigraphy of the Late and Middle Pleistocene coral reef terraces on Southern Barbados (West Indies). *Earth-Science Rev.* **64**, 157–187 (2004).
82. Scoffin, T. P. *et al.* Calcium carbonate budget of a fringing reef on the west coast of Barbados: Part II - Erosion, sediments and internal structure. *Bull. Mar. Sci.* **302**, 457–508 (1980).
83. Montaggioni, L. F. History of Indo-Pacific coral reef systems since the last glaciation: Development patterns and controlling factors. *Earth-Science Rev.* **71**, 1–75 (2005).
84. Hubbard, D. K. Depth-related and species-related patterns of Holocene reef accretion in the Caribbean and western Atlantic: a critical assessment of existing models. *Annu. Meet. Geol. Soc. Am.* 1–18 (2009). doi:doi: 10.1002/9781444312065.ch1
85. Woodroffe, C. D. & Webster, J. M. Coral reefs and sea-level change. *Mar. Geol.* **352**, 248–267 (2014).
86. Camoin, G. F. & Webster, J. M. Coral reef response to Quaternary sea-level and environmental

changes: State of the science. *Sedimentology* **62**, 401–428 (2015).
87. Hibbert, F. D. *et al.* Coral indicators of past sea-level change: A global repository of U-series dated benchmarks. *Quat. Sci. Rev.* **145**, 1–56 (2016).
88. Scoffin, T. P. Taphonomy of coral reefs: a review. *Coral Reefs* **11**, 57–77 (1992).
89. Perry, C. T. Reef Framework Preservation in Four Contrasting Modern Reef Environments, Discovery Bay, Jamaica. *J. Coast. Res.* **15**, 796–812 (1999).
90. Perry, C. T. Storm-induced coral rubble deposition: Pleistocene records of natural reef disturbance and community response. *Coral Reefs* **20**, 171–183 (2001).
91. Blanchon, P. & Perry, C. T. Taphonomic differentiation of Acropora palmata facies in cores from Campeche Bank Reefs, Gulf of Mexico. *Sedimentology* **51**, 53–76 (2004).
92. Perry, C. T. & Hepburn, L. J. Syn-depositional alteration of coral reef framework through bioerosion, encrustation and cementation: Taphonomic signatures of reef accretion and reef depositional events. *Earth-Science Rev.* **86**, 106–144 (2008).
93. Pandolfi, J. M. & Greenstein, B. J. Taphonomic Alteration of Reef Corals: Effects of Reef Environment and Coral Growth Form. I. The Great Barrier Reef. *Palaios* **12**, 27 (1997).
94. Clark, T. R. *et al.* Testing the precision and accuracy of the U-Th chronometer for dating coral mortality events in the last 100 years. *Quat. Geochronol.* **23**, 35–45 (2014).
95. Blanchon, P., Jones, B. & Kalbfleisch, W. Anatomy of a Fringing Reef Around Grand Cayman: Storm Rubble, Not Coral Framework. *J. Sediment. Res.* **67**, 1–16 (1997).
96. Hubbard, D. K. & Miller, A. I. Production and Cycling of Calcium Carbonate in a Shelf-Edge Reef System (St. Croix, U.S. Virgin Islands): Applications to the Nature of Reef Systems in the Fossil Record. *J. Sediment. Res.* **60**, 335–360 (1990).
97. Edinger, E. N., Burr, G. S., Pandolfi, J. M. & Ortiz, J. C. Age accuracy and resolution of Quaternary corals used as proxies for sea level. *Earth Planet. Sci. Lett.* **253**, 37–49 (2007).
98. Marshall, J. F. & Davies, P. J. Internal structure and Holocene evolution of One Tree Reef, southern Great Barrier Reef. *Coral Reefs* **1**, 21–28 (1982).
99. Hopley, D., Smithers, S. G. & Parnell, K. *The Geomorphology of the Great Barrier Reef: Development, Diversity and Change*. (Cambridge University Press, 2007).
100. Long, A. J. *et al.* Near-field sea-level variability in northwest Europe and ice sheet stability during the last interglacial. *Quat. Sci. Rev.* **126**, 26–40 (2015).
101. Rohling, E. J. *et al.* High rates of sea-level rise during the last interglacial period. *Nat. Geosci.* **1**, 38–42 (2008).
102. Cutler, K. B. *et al.* Rapid sea-level fall and deep-ocean temperature change since the last interglacial period. *Earth Planet. Sci. Lett.* **206**, 253–271 (2003).
103. Moseley, G. E., Smart, P. L., Richards, D. A. & Hoffmann, D. L. Speleothem constraints on marine isotope stage (MIS) 5 relative sea levels, Yucatan Peninsula, Mexico. *J. Quat. Sci.* **28**, 293–300 (2013).
104. Hibbert, F. D. *et al.* Coral indicators of past sea-level change: A global repository of U-series dated benchmarks. *Quat. Sci. Rev.* **145**, 1–56 (2016).
105. Grant, K. M. *et al.* Rapid coupling between ice volume and polar temperature over the past 150,000 years. *Nature* **491**, 744–747 (2012).
106. Grant, K. M. *et al.* Sea-level variability over five glacial cycles. *Nat. Commun.* **5**, 5076 (2014).
107. Rohling, E. J. *et al.* Differences between the last two glacial maxima and implications for ice-sheet, δ18O, and sea-level reconstructions. *Quat. Sci. Rev.* **176**, 1–28 (2017).
108. Cheng, H. *et al.* Improvements in ^{230}Th dating, ^{230}Th and ^{234}U half-life values, and U-Th isotopic measurements by multi-collector inductively coupled plasma mass spectrometry. *Earth Planet. Sci. Lett.* **371–372**, 82–91 (2013).
109. Thompson, W. G., Spiegelman, M. W., Goldstein, S. L. & Speed, R. C. An open-system model for U-series age determinations of fossil corals. *Earth Planet. Sci. Lett.* **210**, 365–381 (2003).
110. Gallup, C. D., Cheng, H., Taylor, F. W. & Edwards, R. L. Direct Determination of the Timing of Sea Level Change During Termination II. *Science (80-.).* **295**, 310–313 (2002).
111. Potter, E.-K. *et al.* Suborbital-period sea-level oscillations during marine isotope substages 5a and 5c. *Earth Planet. Sci. Lett.* **225**, 191–204 (2004).
112. Gallup, C. D., Edwards, R. L. & Johnson, R. G. The Timing of High Sea Levels Over the Past

200,000 Years. *Science (80-.).* **263**, 796–800 (1994).
113. Thomas, A. L. *et al.* Penultimate deglacial sea-level timing from Uranium/Thorium dating of Tahitian corals. *Science (80-.).* **324**, 1186–1189 (2009).
114. Stirling, C. H. *et al.* Orbital Forcing of the Marine Isotope Stage 9 Interglacial. *Science (80-.).* **291**, 290–293 (2001).
115. Vesica, P. L. *et al.* Late Pleistocene Paleoclimates and sea-level change in the Mediterranean as inferred from stable isotope and U-series studies of overgrowths on speleothems, Mallorca, Spain. *Quat. Sci. Rev.* **19**, 865–879 (2000).
116. Marino, G. *et al.* Bipolar seesaw control on last interglacial sea level. *Nature* **522**, 197–201 (2015).
117. Irvali, N. *et al.* Rapid switches in subpolar North Atlantic hydrography and climate during the Last Interglacial (MIS 5e). *Paleoceanography* **27**, PA2207 (2012).
118. Irvali, N. *et al.* Evidence for regional cooling, frontal advances, and East Greenland Ice Sheet changes during the demise of the last interglacial. *Quat. Sci. Rev.* **150**, 184–199 (2016).
119. Cox, K. A. Stable isotopes as tracers for freshwater fluxes into the North Atlantic. (University of Southampton, 2010).
120. Cox, K. A. *et al.* Interannual variability of Arctic sea ice export into the East Greenland Current. *J. Geophys. Res.* **115**, C12063 (2010).
121. Dodd, P. A. *et al.* The freshwater composition of the Fram Strait outflow derived from a decade of tracer measurements. *J. Geophys. Res. Ocean.* **117**, C11005 (2012).
122. Rabe, B. *et al.* Liquid export of Arctic freshwater components through the Fram Strait 1998-2011. *Ocean Sci.* **9**, 91–109 (2013).
123. Rohling, E. J. Paleosalinity: confidence limits and future applications. *Mar. Geol.* **163**, 1–11 (2000).
124. Yau, A. M., Bender, M. L., Robinson, A. & Brook, E. J. Reconstructing the last interglacial at Summit, Greenland: Insights from GISP2. *Proc. Natl. Acad. Sci.* **113**, 9710–9715 (2016).
125. Williams, F. H. A geophysical approach to reconstructing past global mean sea levels using highly resolved sea-level records. (University of Southampton, 2016).
126. Dendy, S., Austermann, J., Creveling, J. R. & Mitrovica, J. X. Sensitivity of Last Interglacial sea-level high stands to ice sheet configuration during Marine Isotope Stage 6. *Quat. Sci. Rev.* **171**, 234–244 (2017).
127. Hay, C. C. *et al.* The sea-level fingerprints of ice-sheet collapse during interglacial periods. *Quat. Sci. Rev.* **87**, 60–69 (2014).
128. Kendall, R. A., Mitrovica, J. X. & Milne, G. A. On post-glacial sea level - II. Numerical formulation and comparative results on spherically symmetric models. *Geophys. J. Int.* **161**, 679–706 (2005).
129. Mitrovica, J. X., Wahr, J., Matsuyama, I. & Paulson, A. The rotational stability of an ice-age earth. *Geophyical J. Int.* **161**, 491–506 (2005).
130. Tamisiea, M. E. Ongoing glacial isostatic contributions to observations of sea level change. *Geophys. J. Int.* **186**, 1036–1044 (2011).
131. Stocchi, P. *et al.* MIS 5e relative sea-level changes in the Mediterranean Sea: Contribution of isostatic disequilibrium. *Quat. Sci. Rev.* **185**, 122–134 (2018).
132. Lambeck, K., Rouby, H., Purcell, A., Sun, Y. & Sambridge, M. Sea level and global ice volumes from the Last Glacial Maximum to the Holocene. *Proc. Natl. Acad. Sci. U. S. A.* **111**, 15296–303 (2014).
133. Peltier, W. R. Global glacial isostasy and the surface of the ice-age Earth: the ICE-5G (VM2) model and GRACE. *Annu. Rev. Earth Sci.* **32**, 111–149 (2004).
134. de Boer, B., Stocchi, P. & van de Wal, R. S. W. A fully coupled 3-D ice-sheet–sea-level model: algorithm and applications. *Geosci. Model Dev.* **7**, 2141–2156 (2014).
135. Mao, Y., Economo, E. P. & Satoh, N. The Roles of Introgression and Climate Change in the Rise to Dominance of Acropora Corals. *Curr. Biol.* (2018). doi:10.1016/j.cub.2018.08.061
136. Riegl, B., Berumen, M. & Bruckner, A. Coral population trajectories, increased disturbance and management intervention: a sensitivity analysis. *Ecol. Evol.* **3**, 1050–1064 (2013).
137. Dullo, W.-C. Coral growth and reef growth: a brief review. *Facies* **51**, 33–48 (2005).

138. Morgan, K. M., Perry, C. T., Smithers, S. G., Johnson, J. A. & Gulliver, P. Transitions in coral reef accretion rates linked to intrinsic ecological shifts on turbid-zone nearshore reefs. *Geology* **44**, 995–998 (2016).
139. Perry, C. T. & Morgan, K. M. Bleaching drives collapse in reef carbonate budgets and reef growth potential on southern Maldives reefs. *Sci. Rep.* **7**, 40581 (2017).
140. Perry, C. T., Smithers, S. G., Gulliver, P. & Browne, N. K. Evidence of very rapid reef accretion and reef growth under high turbidity and terrigenous sedimentation. *Geology* **40**, 719–722 (2012).
141. Camoin, G. F., Ebren, P., Eisenhauer, A., Bard, E. & Faure, G. A 300 000-yr coral reef record of sea level changes, Mururoa atoll (Tuamotu archipelago, French Polynesia). *Palaeogeogr. Palaeoclimatol. Palaeoecol.* **175**, 325–341 (2001).
142. Edwards, R. L., Cheng, H., Murrell, M. T. & Goldstein, S. J. Protactinium-231 dating of carbonates by thermal ionization mass\rspectrometry: Implications for Quaternary climate change. *Science (80-.).* **276**, 782–786 (1997).
143. Muhs, D. R., Pandolfi, J. M., Simmons, K. R. & Schumann, R. R. Sea-level history of past interglacial periods from uranium-series dating of corals, Curaçao, Leeward Antilles islands. *Quat. Res.* **78**, 157–169 (2012).
144. Multer, H. G., Gischler, E., Lundberg, J., Simmons, K. R. & Shinn, E. A. Key Largo Limestone revisited: Pleistocene shelf-edge facies, Florida Keys, USA. *Facies* **46**, 229–271 (2002).
145. Speed, R. C. & Cheng, H. Evolution of marine terraces and sea level in the last interglacial, Cave Hill, Barbados. *Geol. Soc. Am. Bull.* **116**, 219–232 (2004).
146. Toscano, M. A. & Lundberg, J. Early Holocene sea-level record from submerged fossil reefs on the southeast Florida margin. *Geology* **26**, 255–258 (1998).
147. Toscano, M. A., Macintyre, I. G. & Lundberg, J. Last interglacial reef limestones, northeastern St. Croix, US Virgin Islands-evidence of tectonic tilting and subsidence since MIS 5.5. *Coral Reefs* **31**, 27–38 (2012).
148. Andersen, M. B. *et al.* The timing of sea-level high-stands during Marine Isotope Stages 7.5 and 9: Constraints from the uranium-series dating of fossil corals from Henderson Island. *Geochim. Cosmochim. Acta* **74**, 3598–3620 (2010).
149. Andersen, M. B. *et al.* High-precision U-series measurements of more than 500,000 year old fossil corals. *Earth Planet. Sci. Lett.* **265**, 229–245 (2008).
150. Bard, E. *et al.* Pleistocene sea levels and tectonic uplift based on dating of corals from Sumba Island, Indonesia. *Geophys. Res. Lett.* **23**, 1473–1476 (1996).
151. Bard, E., Hamelin, B., Fairbanks, R. G. & Zindler, A. Calibration of the ^{14}C timescale over the past 30,000 years using mass spectrometric U–Th ages from Barbados corals. *Nature* **345**, 405–410 (1990).
152. Coyne, M. K., Jones, B. & Ford, D. Highstands during Marine Isotope Stage 5: evidence from the Ironshore Formation of Grand Cayman, British West Indies. *Quat. Sci. Rev.* **26**, 536–559 (2007).
153. Dia, A. ., Cohen, A. ., O'Nions, R. . & Jackson, J. . Rates of uplift investigated through ^{230}Th dating in the Gulf of Corinth (Greece). *Chem. Geol.* **138**, 171–184 (1997).
154. Edwards, R. L., Chen, J. H., Ku, T.-L. & Wasserburg, G. J. Precise Timing of the Last Interglacial Period from Mass Spectrometric Determination of Thorium-230 in Corals. *Science (80-.).* **236**, 1547–1553 (1987).
155. Esat, T. M., McCulloch, M. T., Chappell, J., Pillans, B. & Omura, A. Rapid Fluctuations in Sea Level Recorded at Huon Peninsula During the Penultimate Deglaciation. *Science (80-.).* **283**, 197–201 (1999).
156. Hamelin, B., Bard, E., Zindler, A. & Fairbanks, R. G. $^{234}U/^{238}U$ mass spectrometry of corals: How accurate is the UTh age of the last interglacial period? *Earth Planet. Sci. Lett.* **106**, 169–180 (1991).
157. Ludwig, K. R., Muhs, D. R., Simmons, K. R., Halley, R. B. & Shinn, E. A. Sea-level records at ~ 80 ka from tectonically stable platforms: Florida and Bermuda. *Geology* **24**, 211 (1996).
158. McCulloch, M. T. & Mortimer, G. E. Applications of the $^{238}U–^{230}Th$ decay series to dating of fossil and modern corals using MC-ICPMS. *Aust. J. Earth Sci.* **55**, 955–965 (2008).

159. Muhs, D. R., Simmons, K. R., Kennedy, G. L. & Rockwell, T. K. The last interglacial period on the Pacific Coast of North America: Timing and paleoclimate. *Geol. Soc. Am. Bull.* **114**, 569–592 (2002).
160. Muhs, D. R., Simmons, K. R., Kennedy, G. L., Ludwig, K. R. & Groves, L. T. A cool eastern Pacific Ocean at the close of the Last Interglacial complex. *Quat. Sci. Rev.* **25**, 235–262 (2006).
161. Muhs, D. R. *et al.* Sea-level history during the Last Interglacial complex on San Nicolas Island, California: implications for glacial isostatic adjustment processes, paleozoogeography and tectonics. *Quat. Sci. Rev.* **37**, 1–25 (2012).
162. Stirling, C. H. High-precision U-series dating of corals from Western Australia: implications for last interglacial sea levels. (The Australian National University, 1996).
163. Frank, N. *et al.* Open system U-series ages of corals from a subsiding reef in New Caledonia: Implications for sea level changes, and subsidence rate. *Earth Planet. Sci. Lett.* **249**, 274–289 (2006).
164. McMurtry, G. M., Campbell, J. F., Fryer, G. J. & Fietzke, J. Uplift of Oahu, Hawaii, during the past 500 k.y. as recorded by elevated reef deposits. *Geology* **38**, 27–30 (2010).
165. Zazo, C. *et al.* Quaternary marine terraces on Sal Island (Cape Verde archipelago). *Quat. Sci. Rev.* **26**, 876–893 (2007).
166. Vezina, J., Jones, B. & Ford, D. Sea-level highstands over the last 500,000 years; evidence from the Ironshore Formation on Grand Cayman, British West Indies. *J. Sediment. Res.* **69**, 317–327 (1999).
167. Alley, R. B. *et al.* Oceanic Forcing of Ice-Sheet Retreat: West Antarctica and More. *Annu. Rev. Earth Planet. Sci.* **43**, 207–231 (2015).
168. Bamber, J. L., Oppenheimer, M., Kopp, R. E., Aspinall, W. P. & Cooke, R. M. Ice sheet contributions to future sea-level rise from structured expert judgment. *Proc. Natl. Acad. Sci.* 201817205 (2019). doi:10.1073/pnas.1817205116
169. Cazenave, A. *et al.* Global sea-level budget 1993–present. *Earth Syst. Sci. Data* **10**, 1551–1590 (2018).
170. van den Broeke, M. R. *et al.* On the recent contribution of the Greenland ice sheet to sea level change. *Cryosph.* **10**, 1933–1946 (2016).
171. Capron, E. *et al.* Temporal and spatial structure of multi-millennial temperature changes at high latitudes during the Last Interglacial. *Quat. Sci. Rev.* **103**, 116–133 (2014).
172. Wolff, E. W. *et al.* Southern Ocean sea-ice extent, productivity and iron flux over the past eight glacial cycles. *Nature* **440**, 491–496 (2006).
173. Wolff, E. W. *et al.* Changes in environment over the last 800,000 years from chemical analysis of the EPICA Dome C ice core. *Quat. Sci. Rev.* **29**, 285–295 (2010).
174. Bradley, S. L., Hindmarsh, R. C. A., Whitehouse, P. L., Bentley, M. J. & King, M. A. Low post-glacial rebound rates in the Weddell Sea due to Late Holocene ice-sheet readvance. *Earth Planet. Sci. Lett.* **413**, 79–89 (2015).
175. Gomez, N., Pollard, D. & Mitrovica, J. X. A 3-D coupled ice sheet – sea level model applied to Antarctica through the last 40 ky. *Earth Planet. Sci. Lett.* **384**, 88–99 (2013).
176. Gomez, N., Pollard, D. & Holland, D. Sea-level feedback lowers projections of future Antarctic Ice-Sheet mass loss. *Nat. Commun.* **6**, 8798 (2015).
177. Konrad, H., Sasgen, I., Pollard, D. & Klemann, V. Potential of the solid-Earth response for limiting long-term West Antarctic Ice Sheet retreat in a warming climate. *Earth Planet. Sci. Lett.* **432**, 254–264 (2015).
178. Kingslake, J. *et al.* Extensive retreat and re-advance of the West Antarctic Ice Sheet during the Holocene. *Nature* **558**, 430–434 (2018).